

# Review of Low-Temperature Performance, Modeling and Heating for Lithium-Ion Batteries

Sun, B., Qi, X., Song, D. & Ruan, H.

Published PDF deposited in Coventry University's Repository

**Original citation:**

Sun, B, Qi, X, Song, D & Ruan, H 2023, 'Review of Low-Temperature Performance, Modeling and Heating for Lithium-Ion Batteries', *Energies*, vol. 16, no. 20, 7142.

<https://dx.doi.org/10.3390/en16207142>

DOI 10.3390/en16207142

ISSN 1996-1073

Publisher: MDPI

This article is an open access article distributed under the terms and conditions of the Creative Commons Attribution (CC BY) license

(<https://creativecommons.org/licenses/by/4.0/>)

Review

# Review of Low-Temperature Performance, Modeling and Heating for Lithium-Ion Batteries

Bingxiang Sun <sup>1,\*</sup> , Xianjie Qi <sup>1</sup>, Donglin Song <sup>1,2</sup> and Haijun Ruan <sup>3,4,\*</sup> 

<sup>1</sup> National Active Distribution Network Technology Research Center (NANTEC), Beijing Jiaotong University, Beijing 100044, China

<sup>2</sup> Beijing Aerospace Times Laser Inertial Technology Company, Ltd., Beijing 100094, China

<sup>3</sup> Institute for Clean Growth and Future Mobility, Coventry University, Coventry CV1 5FB, UK

<sup>4</sup> Dyson School of Design Engineering, Imperial College London, London SW7 2AZ, UK

\* Correspondence: bxsun@bjtu.edu.cn (B.S.); haijun.ruan@coventry.ac.uk (H.R.)

**Abstract:** Lithium-ion batteries (LIBs) have the advantages of high energy/power densities, low self-discharge rate, and long cycle life, and thus are widely used in electric vehicles (EVs). However, at low temperatures, the peak power and available energy of LIBs drop sharply, with a high risk of lithium plating during charging. This poor performance significantly impacts the application of EVs in cold weather and dramatically limits the promotion of EVs in high-latitude regions. This challenge recently attracted much attention, especially investigating the performance decrease for LIBs at low temperatures, and exploring the solutions; however, limited reviews exist on this topic. Here, we thoroughly review the state-of-the-arts about battery performance decrease, modeling, and preheating, aiming to drive effective solutions for addressing the low-temperature challenge of LIBs. We outline the performance limitations of LIBs at low temperatures and quantify the significant changes in (dis)charging performance and resistance of LIBs at low temperatures. The various models considering low-temperature influencing factors are also tabulated and summarized, with the modeling improvement for describing low-temperature performance highlighted. Furthermore, we categorize the existing heating methods, and the metrics such as heating rate, energy consumption, and lifetime impact are highlighted to provide fundamental insights into the heating methods. Finally, the limits of current research on low-temperature LIBs are outlined, and an outlook on future research direction is provided.



**Citation:** Sun, B.; Qi, X.; Song, D.; Ruan, H. Review of Low-Temperature Performance, Modeling and Heating for Lithium-Ion Batteries. *Energies* **2023**, *16*, 7142. <https://doi.org/10.3390/en16207142>

Academic Editor: Daniel-Ioan Stroe

Received: 17 August 2023

Revised: 4 October 2023

Accepted: 6 October 2023

Published: 19 October 2023



**Copyright:** © 2023 by the authors. Licensee MDPI, Basel, Switzerland. This article is an open access article distributed under the terms and conditions of the Creative Commons Attribution (CC BY) license (<https://creativecommons.org/licenses/by/4.0/>).

**Keywords:** lithium-ion battery; low temperature; charging; discharging; modeling; heating

## 1. Introduction

With the rapid development of industrialization, the global energy shortage and environmental pollution are becoming increasingly serious, greenhouse gas emissions are increasing year by year, and the awareness of energy saving and environmental protection has become deeply rooted in people's hearts. The theme of electric vehicles (EVs) in today's world is energy saving and environmental protection, and EVs have become the main direction of transformation and development of the global automotive industry and an important engine to promote world economic growth. China released the "New Energy Vehicle Industry Plan", striving to reach the international advanced level of core technology of new energy vehicles by 2035, and the quality brand has strong international competitiveness [1]. According to the regulations previously approved by the EU Council, the sale of non-zero-carbon emission new fuel vehicles will be banned in the EU from 2035 onwards [2]. In 2021, U.S. President Joe Biden signed an executive order proposing that by 2030, the U.S. should achieve a goal of 50% of total new vehicle sales for EVs, aiming to address the threat of climate change [3].

With continued support from national policies and increased public awareness of energy conservation and environmental protection, EVs are growing rapidly. As shown in

Figure 1, from 2015 to 2022, the EV sales share grew 20 times worldwide, which increased by 29 times, grew 17.5 times, and 9.9 times in China, Europe, and America. The global EV sales grew from 0.55 million to 10.2 million [4].

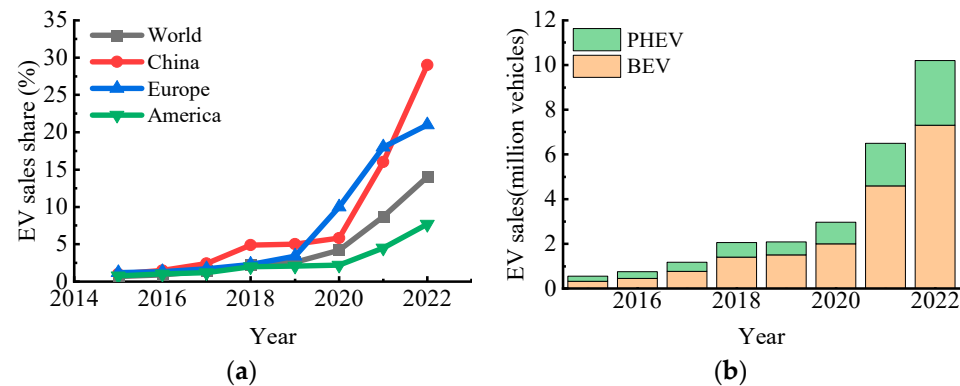


**Figure 1.** 2015–2022, The trend of EVs: (a) Annual EV sales share in China, Europe, America, and the world; EV sales share refers to the ratio of EV sales to the total car sales in a region or country. (b) Annual EV sales in the world [4]. EVs consist of battery electric vehicles (BEVs) and plug-in hybrid electric vehicles (PHEVs).

Compared with traditional lead-acid and nickel–cadmium batteries, lithium-ion batteries (LIBs) are widely used in the field of electric vehicle power drive as a key component because of their advantages such as high energy and power densities, low self-discharge rate, no memory effect, long cycle life, and environmental friendliness. However, the performance of LIBs is greatly reduced at low temperatures. The researchers studied the charging, discharging, electrochemical impedance spectroscopy (EIS), and degradation of LIBs at low temperatures, where the charge transfer kinetics at the LIB interface is hysteretic and the conductivity of the electrolyte is reduced. The solid-phase diffusion of LIBs is slower, which leads to an exponential increase in LIB impedance and a sharp decrease in available energy and peak power, resulting in a sudden decrease in EVs' driving range and hill-climbing performance in low-temperature environments [5] and limited performance in scenarios requiring wide-temperature domain use. Moreover, LIBs suffer from extremely poor charging performance in low-temperature environments, limited at a very small C-rate [6], and it is basically impossible to charge the LIB below  $-10\text{ }^{\circ}\text{C}$ . Compared with the room temperature state, the charging and discharging capacity of the battery is greatly reduced [7]. When the lithium plating reaches a certain level, the generated lithium dendrites will pierce the battery diaphragm, causing the risk of internal short circuit inside the battery, and even cause an explosion, resulting in safety accidents [8].

China accounted for 59% of global EV sales in 2022, cementing its position as the world's largest EVs market. The country is also the world's biggest EVs producer, with 64% of global volume [9]. Therefore, through the Chinese market, we can see the pattern of new energy vehicles in the global market. Winter temperatures in northern China are often below  $0\text{ }^{\circ}\text{C}$ , and even extreme temperatures in some areas can reach  $-30\text{ }^{\circ}\text{C}$  [10]. However, the optimal operating temperature range of LIBs is often considered to be from  $15\text{ to }35\text{ }^{\circ}\text{C}$  [11]. When the operating temperature of LIBs exceeds the optimal operating zone, such as subzero temperatures, the internal electrochemical reaction of the battery becomes slower, the internal resistance becomes larger, and its available capacity and energy are abruptly reduced [12,13]. According to the latest 2022 China EV sales statistics, the amount of EVs' sales in the north of China is quite low, which primarily attributed to the poor performance of LIBs due to the low-temperature regions, as shown in Figure 2. The unevenness of the promotion and application of EVs mainly stems from the problem of wide-temperature domain environmental adaptability of LIBs. Therefore, understanding the poor performance of LIBs in low-temperature environments has become a hot research topic.

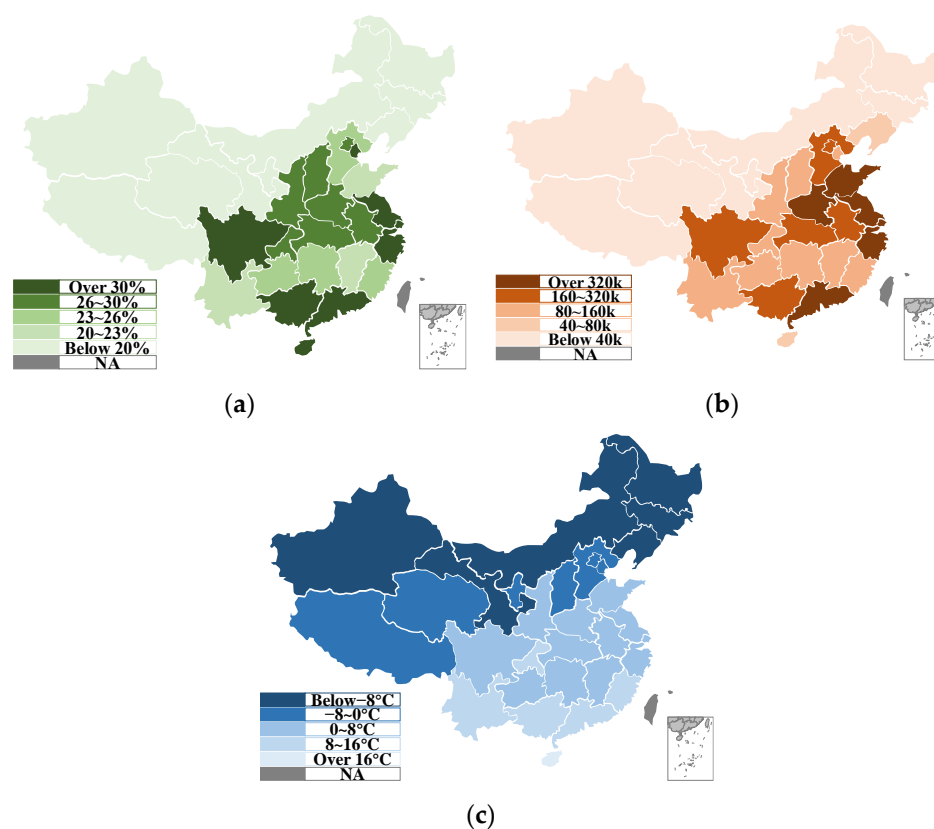


**Figure 2.** The unevenness of EVs promotion and application is partly due to low temperatures: (a) 2022 distribution of EV sales share by provincial capitals in China (EV sales/all-passenger car sales); (b) 2022 distribution of EV sales by province in China; (c) 2020 distribution of average temperature of the lowest month in each provincial capital city in China [10]. The source of the data on temperatures is the China Meteorological Yearbook 2021, with only 2020 data currently publicly available, and the temperature variations from year to year in the same area are small and therefore have less impact on drawing relevant conclusions.

In addition to studying the performance of batteries at low temperatures, researchers have also investigated the low-temperature models of batteries. The accuracy of LIB models directly affects battery state estimation, performance prediction, safety warning, and other functions. Commonly used battery models work well at room/high temperatures, but their accuracy decreases significantly at low temperatures. By improving traditional models for application in low-temperature environments, researchers can more accurately simulate the battery operating state at low temperature. At the same time, the electrothermal coupling behavior of the battery in the low-temperature environments will directly affect the accuracy of the battery model, and the establishment of the electrothermal coupling model is essential to accurately describe the low-temperature characteristics of the battery.

Finally, plenty of efforts have been made to restore the performance of batteries at low temperatures, and two main methods are currently used: (1) Improving the positive and negative electrode materials or electrolyte materials [14]. Improvement of low-temperature performance of LIBs involves various aspects. Currently, research on electrolytes mainly focuses on modifying solvents and lithium salts, adding a small amount of organic compounds, or combining modification methods. Research on electrode materials mainly focuses on metal or nonmetal doping, surface coating, and morphology control. There are also studies on other battery components such as separators, binders, and conductive agents. The purpose of these studies is to improve the low-temperature performance of LIBs. However, there are many factors affecting the low-temperature performance of LIBs, which is a complex systematic problem, and improved electrode materials can only

meet part of the performance requirements of LIBs. High-performance electrode materials that can balance cost, energy density, and safety performance are difficult to achieve in a short time. (2) Preheating the battery. Since the performance degradation of LIBs at low temperatures is recoverable, that is, if the operating temperature of the battery is raised to room temperature (RT), the performance of the LIB will be restored to the level at RT. LIB low-temperature heating technology is well adapted to meet the use of power batteries under low-temperature conditions, and it is also the mainstream solution to solve the problem of low-temperature LIBs. At present, research on the classification methods of low-temperature heating for LIBs [15,16] mainly includes the internal heating method, external heating method, and hybrid heating method.

The effect of low temperatures on LIBs is extremely important, but limited studies have thoroughly investigated this, as presented in Tables 1–3, there are limited reviews related to this topic, and the available reviews only briefly cover a portion of the topic; no comprehensive review has been conducted. For the convenience of the readers, the existing review papers and comments on the existing battery models and the low-temperature heating technologies are listed in Tables 1 and 2. In addition, a comprehensive examination of review papers on low-temperature LIB materials is given in Table 3. To fill in the gaps, the review aims to quantify, and provide a sound research basis for existing low-temperature performance investigation, modelling, and preheating technologies, with the goal of the motivation of new solutions and the identification of research gaps, as well as future directions.

**Table 1.** Battery modeling review paper and its main content.

Key Words	Focus of Literature	Year	Ref.
• Porous electrode model	Modeling and Optimization; Overpotential and impedance; Temperature and stress; Aging	2022	[17]
• Physics-based LIBs models	Microscale model; Doyle–Fuller–Newman model; Single-particle model; Coupled thermal–electrochemical models	2022	[18]
• High-fidelity model	Reconstructed electrochemical modeling; Simplified electrochemical modeling; Thermal modeling; Electrochemical–thermal coupling modeling	2022	[19]
• Pseudo-two-dimensional (P2D) model	P2D model and simplifications; Extension of P2D model; P2D model parameterization	2022	[20]
• Neural network model	Kalman filter-first method; Neural-network-first method	2022	[21]
• Fractional-order model	Frequency-domain modelling; Time-domain modelling	2020	[22]

**Table 2.** Low-temperature heating technology review paper and its main content.

Key Words	Focus of Literature	Year	Ref.
• Essential problems at low temperature (LT)	Mechanisms; Potential; Maturity; Pros and cons	2020	[23]
• External heating	Mutual pulse heating; Self-heating lithium-ion battery (SHLB); Alternating current (AC) heating; Convective and conductive heating; Internal self-heating		
• Internal heating	Mechanisms; Potential; Pros and cons		
	Mechanisms; Potential; Applications; Pros and cons;	2022	[24]
		2022	[25]
• Performance at LT	Mechanisms, Pros and cons	2022	[26]
• Research base at LT	Mutual pulse current heating; AC heating; Compound heating;		
• Internal Heating	All-climate-battery-based heating;		
• Self-heating	Present the heating triangle to quantitatively assess self-heating methods	2023	[27]

**Table 3.** Low-temperature battery materials review paper and its main content.

Key Words	Focus of Literature	Year	Ref.
<ul style="list-style-type: none"> <li>Essential problems at LT</li> <li>Anodes at LT</li> <li>Cathodes at LT</li> <li>Electrolytes at LT</li> </ul>	Battery configurations; Obtained LT performances	2023	[28]
<ul style="list-style-type: none"> <li>Failure mechanism at LT</li> <li>Electrolytes at LT</li> <li>Novel electrolytes at LT</li> <li>Anodes at LT</li> </ul>	LiFePO <sub>4</sub> -based batteries (LFP)	2022	[29]
<ul style="list-style-type: none"> <li>Sluggish surface/interface processes at LT</li> <li>Surface/interface modification</li> </ul>	Surface coating; Surface doping; Solid electrolyte interphase (SEI)-forming electrolyte additives	2023	[30]
<ul style="list-style-type: none"> <li>Main factors limiting at LT</li> <li>Electrolytes at LT</li> </ul>	Electrolyte solvents; Additives; Lithium salts; New strategies for LT electrolyte	2023 2022 2022	[31] [32] [33] [34]
<ul style="list-style-type: none"> <li>Performance at LT</li> <li>LT Storage System</li> </ul>	Li <sup>+</sup> Transport in Electrolyte; Desolvation Process; SEI/Cathode Electrolyte Interphase (CEI); Electrode Dynamic	2023	[35]
<ul style="list-style-type: none"> <li>Limitations of LIBs at LT</li> <li>Electrodes at LT</li> </ul>	-	2023	[36]
<ul style="list-style-type: none"> <li>Graphite anode and electrolyte at LT</li> <li>Structural regulation of LT graphite anode</li> </ul>	-	2022	[37]
<ul style="list-style-type: none"> <li>Aging of LIB at LT</li> <li>Electrodes, separators, electrolytes at LT</li> </ul>	Calendar aging; Cycle aging	2022	[38]
<ul style="list-style-type: none"> <li>Cathodes of LIB at LT</li> </ul>	Polyanion and oxide cathode	2022	[39]
<ul style="list-style-type: none"> <li>Discharge performance at LT</li> <li>Electrolytes at LT</li> <li>Electrodes at LT</li> </ul>	-	2022	[40]
<ul style="list-style-type: none"> <li>Main factors limiting LT performance</li> <li>Anodes at LT</li> <li>Cathodes at LT</li> </ul>	Battery configurations; Obtained LT performances	2022	[41]
<ul style="list-style-type: none"> <li>Nonaqueous liquid electrolyte</li> <li>Electrolyte/electrode interphase at LT</li> <li>Binders at LT</li> </ul>	Methods; Materials; Mechanisms	2022 2022 2021	[42] [43] [44]
<ul style="list-style-type: none"> <li>Electrolyte and anode at LT</li> <li>Key issues for cathodes at LT</li> <li>Improving kinetics of cathodes at LT</li> <li>C-rates on capacity and polarization at LT</li> </ul>	-	2022	[45]
<ul style="list-style-type: none"> <li>Electrolyte and anode at LT</li> <li>Key issues for cathodes at LT</li> <li>Improving kinetics of cathodes at LT</li> <li>C-rates on capacity and polarization at LT</li> </ul>	LFP and Li <sub>3</sub> V <sub>2</sub> (PO <sub>4</sub> ) <sub>3</sub> (LVP) phosphate cathode materials; Layered LiCoO <sub>2</sub> (LCO), LiNi <sub>1-x-y</sub> Co <sub>x</sub> MnyO <sub>2</sub> (NCM) and LiNi <sub>1-x-y</sub> Co <sub>x</sub> Al <sub>y</sub> O <sub>2</sub> (NCA) oxide cathode materials; Li- and Mn-rich oxide cathode materials	2022	[46]
<ul style="list-style-type: none"> <li>Anodes at LT</li> <li>Electrolytes at LT</li> <li>Cathodes at LT</li> <li>Heating</li> </ul>	-	2022	[47]
<ul style="list-style-type: none"> <li>Anodes at LT</li> <li>Electrolytes at LT</li> <li>Cathodes at LT</li> <li>Heating</li> </ul>	-	2020	[48]
<ul style="list-style-type: none"> <li>Performance at LT</li> <li>Limitations of now cells</li> <li>Anodes at LT</li> </ul>	Carbon-based anodes; Lithium metal anodes; Titanium-based anodes; Li alloying anodes; Composite anodes	2021	[49]
<ul style="list-style-type: none"> <li>Electrolytes at LT</li> <li>Cathodes and CEI at LT</li> <li>Anodes and SEI at LT</li> <li>Binders at LT</li> </ul>	-	2020	[50]

The remainder of the paper is organized as follows. Section 2 summarizes the impact of low temperature on batteries from a performance perspective. Sections 3 and 4 describe

the modeling and heating strategies for batteries at low temperatures, respectively, followed by Section 5 with conclusions and perspectives.

## 2. Low-Temperature Performance

The charge–discharge performance and lifetime of LIBs at low temperatures are seriously decreased [51,52]. Furthermore, charging at low temperatures likely leads to lithium deposition, and the resulting lithium dendrites may puncture the separator and cause internal short circuits, resulting in safety problems. Therefore, it is of great significance to study the performance of LIB at low temperatures. In this section, the performance of LIB at low temperatures is reviewed from four perspectives: charging, discharging, EIS, and degradation.

### 2.1. Charging

Battery performance can be expressed in terms of a number of parameters, one of the main indicators being the capacity. The capacity is the amount of electricity that can be charged or discharged from a battery under certain conditions (a certain charge/discharge rate, a certain temperature, a certain cut-off voltage, etc.) and is measured in Ah.

To understand the charging performance changes of LIBs at low temperatures, we collected the data reported in the literature, as shown in Table 4, which lists the quantified capacity drop and the increased mid-point voltage (nominal and charging capacity) of different batteries under different conditions. The charging capacity of LIBs at low temperatures decreases as the temperature drops. For example, Zhang et al. [53] reported that the charging capacity of the battery at  $-20\text{ }^{\circ}\text{C}$  and  $-30\text{ }^{\circ}\text{C}$  drops to 93.65% and 87.92%, respectively, compared to those at room temperature. They suggested that the low charging capacity is primarily attributed to the dramatic decrease in ionic conductivity of the electrolyte and the resulting increased SEI resistance at low temperatures. Ren et al. [54] found experimentally that at  $-5\text{ }^{\circ}\text{C}$ , the batteries exhibited no significant capacity loss when charged at 1/6 C-rate, whereas when charged with currents of larger than 1/3 C-rate, the batteries exhibited significant capacity loss, up to 86.51% at 1 C-rate and 81.53% at 2 C-rate. Singer et al. [55] suggested that the capacity fading was caused by lower ionic conductivity, which results in an increase in the internal resistance. However, at very low C-rates, the lower ionic conductivity is not the main reason for the capacity drop. The high activation energies  $E_a$  and the difference in activation energy  $E_a$  between the cathode and anode are the reasons for low-temperature-induced capacity fade at low currents. This element will be further explained in detail in Section 2.2.

**Table 4.** Changes in charging capacity and midpoint voltage of different batteries at low temperatures.

Nominal Capacity (Ah)	Battery Type	Material	Charging Current	T ( $^{\circ}\text{C}$ )	Charging Capacity (%)	Midpoint Voltage (Charging Capacity) (V)	Midpoint Voltage (Nominal Capacity) (V)	Ref.
-	Lab-made	-	0.1 mA/cm <sup>2</sup>	RT <sup>a</sup> -20 -30	100.00 93.65 87.92	0.143 0.341 0.520	0.143 <sup>b</sup> 0.345 <sup>b</sup> 0.531 <sup>b</sup>	[53]
2.300	High-quality Cylindrical 26650	LFP	0.05 C-rate	RT <sup>a</sup> 0 -18	100.00 102.64 96.58	3.325 3.329 3.323	3.327 3.331 3.324	[56]
5.000	High-energy 21700	NCA + LNO	0.4 C-rate	RT <sup>a</sup> 15 0 -10	100.00 92.62 88.03 80.60	3.926 3.888 3.956 4.02	3.953 3.945 4.006 4.082	[57]
0.100	Lab-made Pouch	NCM	0.5 C-rate	RT <sup>a</sup> 15 5 0 -5 -15	100.00 96.82 96.26 90.57 90.07 86.06	3.748 3.762 3.813 3.817 3.849 3.937	3.758 3.781 3.834 3.856 3.888 3.984	[57]

Table 4. Cont.

Nominal Capacity (Ah)	Battery Type	Material	Charging Current	T (°C)	Charging Capacity (%)	Midpoint Voltage (Charging Capacity) (V)	Midpoint Voltage (Nominal Capacity) (V)	Ref.
24.000	Pouch	NCM/LiC	1/6 C-rate 1/3 C-rate 2/3 C-rate 1 C-rate 2 C-rate	−5	100.00 96.80 93.00 86.51 81.53	3.790 3.888 3.976 4.047 4.176	3.800 3.898 3.992 4.068 4.200 <sup>c</sup>	[54]
-	Lab-made	LVP	0.1 C-rate	RT <sup>a</sup> 0 −20	100.00 86.60 67.86	3.953 3.864 4.133	3.953 <sup>b</sup> 4.098 <sup>b</sup> 4.150 <sup>b</sup>	[58]
3.400	Cylindrical	NCA/LiC	0.1 C-rate	RT <sup>a</sup> 0 −10 −20	100.00 88.98 77.65 52.70	3.710 3.754 3.789 3.997	3.725 3.810 3.900 4.180	
1.100	Cylindrical	LFP/LiC	0.1 C-rate	RT <sup>a</sup> 0 −10 −20	100.00 95.13 87.41 67.73	3.324 3.348 3.386 3.472	3.326 3.350 3.400 3.510	[55]
0.130	Pouch	LFP/LTO	0.1 C-rate	RT <sup>a</sup> 0 −10 −20	100.00 76.16 34.95 3.51	1.890 1.904 1.971 2.062	1.890 1.909 - -	
10.000	Prismatic	LMO/LTO	0.1 C-rate	RT <sup>a</sup> 0 −10 −20	100.00 98.68 97.74 93.97	2.489 2.487 2.486 2.496	2.489 2.492 2.497 2.502	
-	Lab-made	NCM	25 mA/g	RT <sup>a</sup> 10 0	100.00 84.50 61.78	4.487 4.483 4.346	4.487 <sup>b</sup> 4.523 <sup>b</sup> 4.560 <sup>b</sup>	[59]
0.140	Coin-type 2032	LCO	0.1 C-rate 0.2 C-rate 0.5 C-rate 1 C-rate 2 C-rate	RT <sup>a</sup>	100.00 98.59 96.67 92.29 83.85	3.734 3.736 3.737 3.747 3.771	3.726 3.730 3.736 3.760 3.818	[60]
			0.1 C-rate 0.2 C-rate 0.5 C-rate	−20	97.15 64.73 50.92	3.921 3.959 4.050	3.917 4.134 4.200 <sup>c</sup>	

<sup>a</sup> 20~25 °C; <sup>b</sup> Use room temperature charging capacity as the nominal capacity; <sup>c</sup> Cut-off voltage. LiNiO<sub>2</sub> (LNO); LiMn<sub>2</sub>O<sub>4</sub> (LMO); Li<sub>4</sub>Ti<sub>5</sub>O<sub>12</sub> (LTO).

Regarding the charging voltage, the midpoint voltage of the cell, which indicates the voltage at the half nominal capacity, increases as the temperature decreases. For example, the midpoint voltages at −20 °C and 0 °C are 197 mV and 145 mV higher than those at room temperature, respectively. Qiao et al. [58] attribute this to the increased cell polarization. According to the different mechanisms of polarization voltage generation, it can be divided into electrochemical polarization voltage and concentration polarization voltage. In low-temperature environments, the electrochemical reaction speed is affected more while the electron transport speed in the external circuit is less affected, which leads to the increase of electrochemical polarization; similarly, the diffusion speed of lithium ions in the electrolyte and active material particles are affected to a certain extent, which leads to the increase of concentration polarization. Both polarization voltages are essentially due to the fact that the rate of movement of lithium ions back and forth between the positive and negative electrodes is affected by temperature, resulting in an imbalance in the concentration of ions inside the battery for a short period of time, resulting in a potential difference to the outside, and this phenomenon becomes more pronounced as the temperature decreases, directly governing the charge and discharge characteristics of the battery.

In Figure 3a, we can see that the rate of reduction in capacity becomes greater as the temperature decreases. For example, the cells in [58] showed a 13.4% drop in capacity at 0 °C, while a 32.14% drop in capacity at −20 °C compared to that at room temperature.

In Figure 3b, we can conclude that the charging capacity of the battery is less affected by temperature when the battery was charged with low currents, such as at 0.1 C-rate. However, when the charging current is increased, such as at 0.2 C-rate, the charging capacity decreases significantly at low temperatures. In Figure 3c, it can be observed that the midpoint voltages of the cell under different currents are almost unchanged at room temperature. However, at low temperatures, the midpoint voltage of the battery increases as the charging current rises, the midpoint voltage at  $-20\text{ }^{\circ}\text{C}$  and 0.1 C-rate is 105% of that at room temperature at 0.1 C-rate. This may be due to the enhanced polarization of the battery at low temperatures, resulting in less energy being charged. The above results show that the high C-rate charging at low temperatures likely causes the battery to reach its cut-off voltage in a shorter period of time, and the charged energy is thus less.

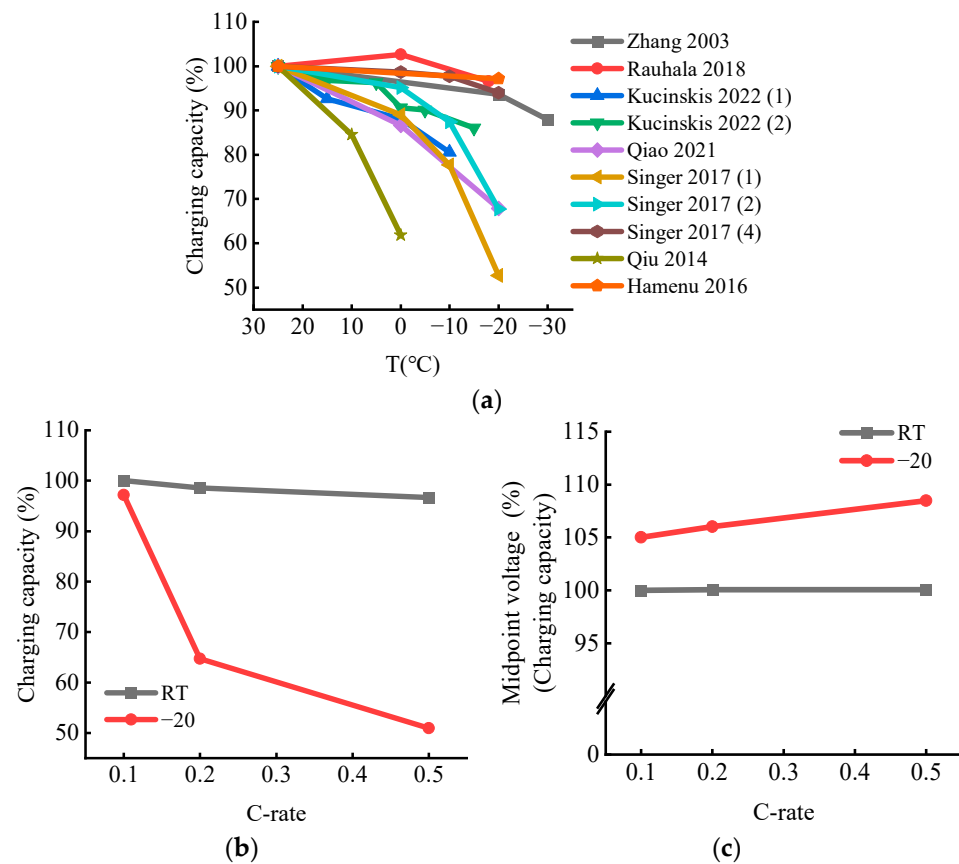


**Figure 3.** Charging performance of low-temperature LIBs: (a) Normalized charging capacity of batteries under different temperatures [53,55–60]; (b) Charging capacity of batteries under different C-rates and different temperatures [60]; (c) Midpoint voltage (charging capacity) of batteries under different C-rates [60].

## 2.2. Discharging

The discharging performance of the battery is related to the EV's range. The more the EV's battery's discharging capacity decreases at low temperatures, the shorter its range. Additionally, the decreasing trend of discharging capacity at low temperatures is very similar to the charging capacity.

To understand the discharging performance changes of LIBs at low temperatures, we collected the data reported in the literature, as shown in Table 5, which lists the quantified capacity drop of different batteries under different conditions. Chen et al. [61] developed an experimental facility to measure the battery discharge characteristics accurately through precise control of operating temperatures utilizing a water–ethylene glycol solution in a constant-temperature thermal bath. Experimental results showed that the measured capacity of the battery is higher when using the conventional air convection temperature

control method due to the higher temperature achieved by the battery during the course of testing with an increase in capacity of 25%, 12%, and 18% for 1 C-rate, 2 C-rate, and 3 C-rate discharge rates, respectively. The results obtained are not representative of the true battery discharge characteristics at the set temperature due to the increase in battery temperature from battery internal heat generation.

**Table 5.** Discharging performance of different batteries at low temperatures.

Nominal capacity (Ah)	6.000	0.140	20.000	100.000	0.023	-	3.400	1.100	0.130	10.000
Cathode	-	LCO	LFP	LFP	NCM	LVP	NCA	LFP	LFP	LMO
Anode	-	-	-	-	-	-	LiC	LiC	LTO	LTO
Ref.	[62]	[60]	[61]	[63]	[64]	[58]		[55]		
T (°C)	C-rate	Discharging capacity (%) <sup>a</sup>								
RT <sup>b</sup>	0.1	-	100.00	-	-	-	100.00	100.00	100.00	100.00
	0.2	100.00 <sup>c</sup>	96.55	100.00	-	-	99.91	-	-	-
	0.5	-	92.76	94.77	100.00	100.00 <sup>e</sup>	99.82	-	-	-
	1	94.65	-	89.86	97.02	99.03 <sup>f</sup>	99.74	-	-	-
	2	84.10	-	81.93	-	-	99.56	-	-	-
0	0.1	-	-	-	-	-	85.34	88.95	97.00	81.99
	0.2	86.42 <sup>c</sup>	-	81.54	-	-	85.08	-	-	-
	0.5	-	-	69.10	78.81	99.07 <sup>e,g</sup>	84.70	-	-	-
	1	78.47	-	57.05	77.15	98.06 <sup>f,g</sup>	83.74	-	-	-
	2	68.64	-	40.89	-	-	82.17	-	-	-
-10	0.1	-	-	-	-	-	-	81.43	91.67	35.83
	0.2	-	-	64.03	-	-	-	-	-	-
	0.5	-	-	47.86	74.50	-	-	-	-	-
	1	-	-	32.96	74.83	-	-	-	-	-
	2	-	-	10.46	-	-	-	-	-	-
-20	0.1	-	63.79	-	-	-	67.16	49.69	65.68	3.49
	0.2	63.29 <sup>c,d</sup>	51.72	-	-	-	61.71	-	-	-
	0.5	-	19.66	-	60.60	-	54.30	-	-	-
	1	56.50 <sup>d</sup>	-	-	71.19	-	33.97	-	-	-
	2	26.88 <sup>d</sup>	-	-	-	-	23.37	-	-	-

<sup>a</sup> We take the discharging capacity at room temperature and low C-rate as the maximum discharging capacity of batteries; <sup>b</sup> 20~25 °C; <sup>c</sup> 1/3 C-rate; <sup>d</sup> -18 °C; <sup>e</sup> 0.65 C-rate; <sup>f</sup> 1.3 C-rate; <sup>g</sup> 5 °C.

Singer et al. [55] suggested that the capacity fading was, on the one hand, caused by lower ionic conductivity, which results in an increase of the internal resistance, but at very low C-rates, the effect of lower ionic conductivity did not dominate; namely, that high activation energies  $E_a$  and the difference in activation energy  $E_a$  between the cathode and the anode are the reasons for low-temperature-induced capacity fade at low currents. They considered that, on the one hand, cell (4) (Cathode: LMO; Anode: LTO) has the lowest activation energy  $E_{a,anode}$  and  $E_{a,cathode}$ , which results in the best low temperature performance. On the other hand, cell (3) (Cathode: LFP; Anode: LTO) has the highest activation energy  $E_{a,cathode}$  and thus the worst performance. Cell (3) and cell (4), the anode of both which are LTO materials, differ significantly in their performance at low temperatures due to the different electrode design. The activation energies of cells (1)–(4) are shown in Table 6.

**Table 6.** Different cathodic and anodic activation energies of cells (1)–(4) as well as corresponding activation factors  $f_a$  [55].

Cell No.	Cell (1)	Cell (2)	Cell (3)	Cell (4)
Anode	LiC	LiC	LTO	LTO
Cathode	NCA	LFP	LFP	LMO
Nominal capacity (Ah)	3.40	1.10	0.13	10.00
Battery type	Cylindrical	Cylindrical	Pouch	Prismatic
$E_{a,cathode}$ (kJ/mol)	39.6	38.5	46.3	10.2
$E_{a,anode}$ (kJ/mol)	19.7	21.1	19.6	9.5
$f_a$	0.50	0.45	0.58	0.07

In Figure 4a, we can see that the discharging capacity decreases at a greater rate as the temperature drops. For example, Jaguemont et al. [63] presented that the discharging capacity of the battery at 0.5 C-rate at 0 °C and −20 °C drops to 78.81% and 60.60%, respectively, compared to those at room temperature. In Figure 4b, we can see that when the battery is discharged at 1/3 C-rate, the discharging capacity decreases as the temperature drops. At 0 °C, the battery was still able to maintain more than 80% of its discharging capacity at room temperature, but at −20 °C, it has dropped to 63.29% (already reaching the retirement standard).

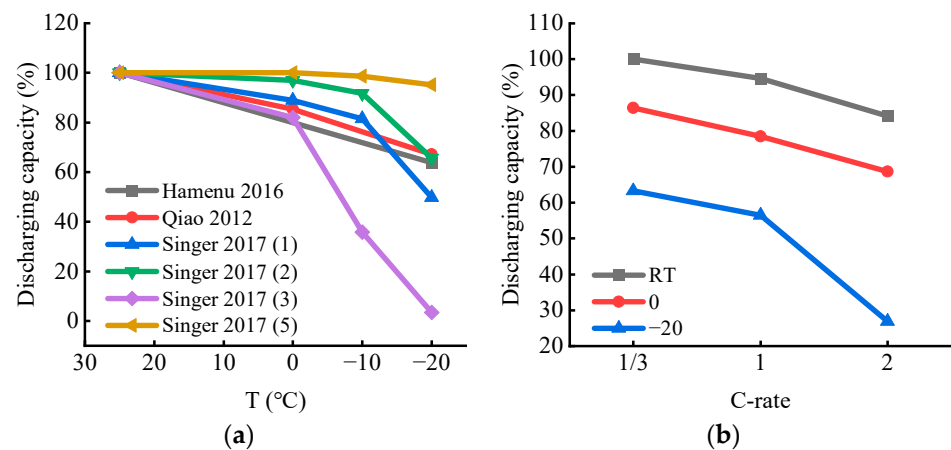


**Figure 4.** Low-temperature LIB discharging performance: (a) Normalized discharging capacity of batteries under different temperatures (0.1 C-rate) [55,58,60]; (b) Discharging capacity of batteries under different temperatures and C-rates [62].

Lowering the temperature and increasing the discharge current would lead to an increased reduction in battery discharging capacity. At 1 C-rate and 0 °C, the voltage drop due to the increase in internal resistance has reduced the battery capacity to 78.47% (the retirement criterion for EVs has been reached).

### 2.3. Resistance (EIS)

EIS is a commonly used noninvasive method to gain a more profound understanding of internal information of LIBs. The Nyquist plots from the EIS test of the cells are illustrated in Figure 5a, which could be fitted to an equivalent circuit model (ECM) to describe the kinetic processes with resistance elements, capacitive elements, and Warburg impedance.

As shown in Figure 5a, three characteristic points are introduced in this paper. The characteristic point **a** is located at the intersection between the EIS curve and the  $x$ -axis, and the highest point of the semicircle is point **b**, with the lowest point at the end of the semicircle being point **c**.

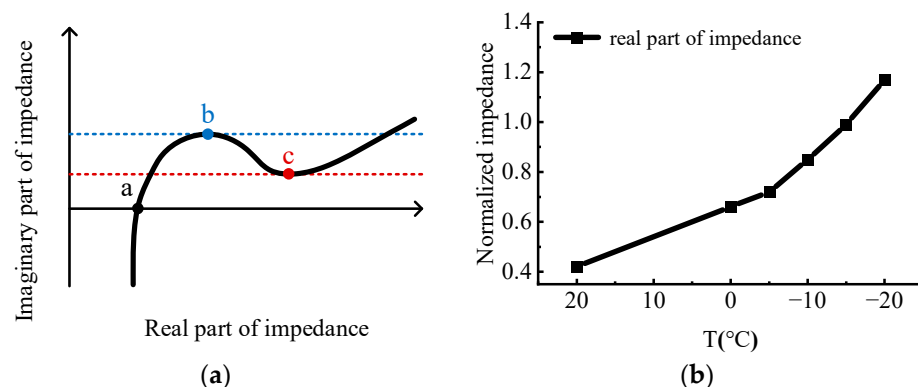


**Figure 5.** Cont.

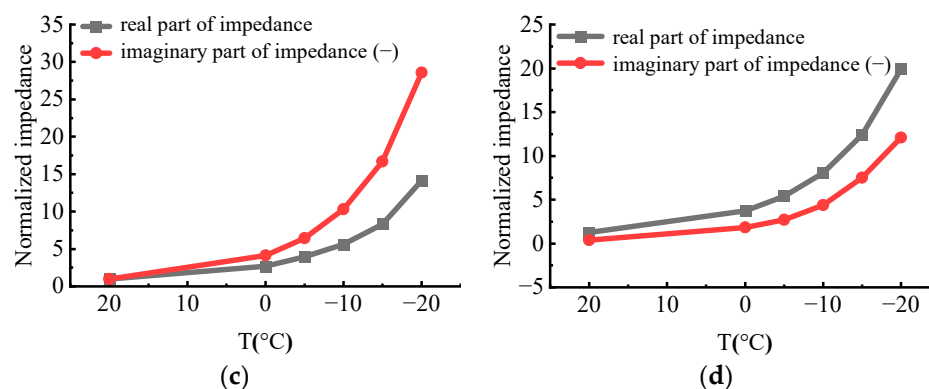


**Figure 5.** Changes in EIS characteristic points at low temperatures for different LIBs: (a) Nyquist chart for EIS testing; (b) Changes in real part of impedance of point a under different temperatures; (c) Changes in real and imaginary parts of impedance of point b under different temperatures; (d) Changes in real and imaginary parts of impedance of point c under different temperatures [65]. We take the point b at room temperature as the benchmark.

In order to understand in more detail how the EIS characteristic points change for LIBs at low temperatures, they are tabulated and detailed. Table 7 lists the relevant literature, including cell capacity, cell type, cell material, experimental temperature, and the relative position of points a, b, c (We take the point b at room temperature as the benchmark).

**Table 7.** Changes in EIS characteristic points at low temperatures for different LIBs.

Nominal Capacity (Ah)	Battery Type	Material	SOC	T (°C)	Point a	Point b <sup>a</sup>	Point c	Ref.
3.100	18650	-	0.2 C-rate <sup>d</sup> 0.5 C-rate <sup>d</sup> 1 C-rate <sup>d</sup>	-10	(0.81, 0) <sup>b</sup> (0.95, 0) <sup>b</sup> (1.15, 0) <sup>b</sup>	(1.00, 1.00) <sup>b</sup> (1.09, 0.73) <sup>b</sup> (1.33, 0.57) <sup>b</sup>	(1.16, 0.50) <sup>b</sup> (1.21, 0.40) <sup>b</sup> (1.39, 0.41) <sup>b</sup>	[66]
-	-	NCM	50% 50% 50% 90% 100%	25 10 -5 -15 0	(0.66, 0) (0.81, 0) (1.23, 0) (1.23, 0) (0.96, 0) (0.96, 0)	(1.00, 1.00) (2.54, 4.15) (12.31, 28.34) (35.36, 85.35) (6.73, 14.03) (8.82, 17.66)	(1.32, 0.14) (4.19, 0.69) (23.83, 3.62) (67.96, 11.99) (12.30, 2.18) (16.81, 4.74)	[67]
2.300	High-quality Cylindrical 26650	LFP	-	RT 0 -18	(0.87, 0) (0.83, 0) (0.85, 0)	(1.00, 1.00) (0.94, 0.80) (1.01, 1.04)	(1.24, 0.53) (1.12, 0.50) (1.23, 0.59)	[56]
0.800	-	-	-	20 0 -5 -10 -15 -20	(0.42, 0) (0.66, 0) (0.72, 0) (0.85, 0) (0.99, 0) (1.17, 0)	(1.00, 1.00) (2.68, 4.14) (3.94, 6.45) (5.61, 10.32) (8.32, 16.68) (14.15, 28.56)	(1.24, 0.40) (3.71, 1.84) (5.39, 2.72) (8.05, 4.39) (12.43, 7.50) (19.91, 12.10)	[65]
1.000	-	-	-	5 0 -5 -10 -15 -20	(0.23, 0) <sup>c</sup> (0.26, 0) <sup>c</sup> (0.30, 0) <sup>c</sup> (0.30, 0) <sup>c</sup> (0.33, 0) <sup>c</sup> (0.36, 0) <sup>c</sup>	(1.00, 1.00) <sup>c</sup> (1.51, 1.69) <sup>c</sup> (2.29, 3.07) <sup>c</sup> (4.00, 5.54) <sup>c</sup> (6.32, 10.14) <sup>c</sup> (11.38, 18.74) <sup>c</sup>	(1.65, 0.28) <sup>c</sup> (2.46, 0.50) <sup>c</sup> (4.10, 0.90) <sup>c</sup> (6.82, 1.98) <sup>c</sup> (11.27, 4.65) <sup>c</sup> (19.14, 11.61) <sup>c</sup>	[68]
3.000	18650	NCM	-	23 <sup>f</sup> 10 <sup>f</sup> 0 <sup>f</sup> -10 <sup>f</sup>	(0.79, 0) <sup>e</sup> (1.32, 0) <sup>e</sup> (1.58, 0) <sup>e</sup> (1.80, 0) <sup>e</sup>	(1.00, 1.00) <sup>e</sup> (1.62, 1.63) <sup>e</sup> (1.93, 2.51) <sup>e</sup> (2.29, 3.30) <sup>e</sup>	(1.14, 0.48) <sup>e</sup> (1.86, 0.68) <sup>e</sup> (2.39, 1.04) <sup>e</sup> (2.85, 1.08) <sup>e</sup>	[69]
2.600	18650	NCA	-	23 <sup>f</sup> 10 <sup>f</sup> 0 <sup>f</sup> -10 <sup>f</sup>	(0.60, 0) <sup>e</sup> (0.59, 0) <sup>e</sup> (0.93, 0) <sup>e</sup> (0.74, 0) <sup>e</sup>	(1.00, 1.00) <sup>e</sup> (0.90, 0.67) <sup>e</sup> (1.23, 1.00) <sup>e</sup> (1.02, 0.90) <sup>e</sup>	(1.25, 0.78) <sup>e</sup> (1.06, 0.48) <sup>e</sup> (1.49, 0.37) <sup>e</sup> (1.21, 0.29) <sup>e</sup>	[69]
1.500	18650	NCM	-	23 <sup>f</sup> 10 <sup>f</sup> 0 <sup>f</sup> -10 <sup>f</sup>	(0.37, 0) <sup>e</sup> (0.37, 0) <sup>e</sup> (0.37, 0) <sup>e</sup> (0.37, 0) <sup>e</sup>	(1.00, 1.00) <sup>e</sup> (1.30, 1.50) <sup>e</sup> (1.58, 1.94) <sup>e</sup> (1.00, 1.00) <sup>e</sup>	(1.66, 0.67) <sup>e</sup> (2.23, 0.96) <sup>e</sup> (2.66, 1.11) <sup>e</sup> (1.56, 0.72) <sup>e</sup>	[69]

<sup>a</sup> We take the point b at room temperature as the benchmark; <sup>b</sup> Point b at 0.2 C-rate and -10 °C as the benchmark; <sup>c</sup> Point b at 5 °C as the benchmark; <sup>d</sup> Cycles at the C-rate; <sup>e</sup> EIS test at room temperature; <sup>f</sup> Cycles at the temperature.

Point **a** moves to the right with decreasing temperature, indicating an increase in ohmic resistance, which is mainly related to the reduced conductivity of the electrolyte. As shown in Figure 5b, the real impedance at point **a** increases near linearly with the decreasing temperature, with the ohmic resistance at  $-20\text{ }^{\circ}\text{C}$  being 278.6% of that at  $20\text{ }^{\circ}\text{C}$ . As the temperature decreases, point **b** moves to the right, and the charge transfer impedance increases, which is associated with sluggish kinetic processes [66]. At the same time, point **c** also shifts to the right, which represents the diffusion process becoming slower at lower temperatures.

As shown in Figure 5c,d, unlike the change at point **a**, the change in impedance at points **b** and **c** increases exponentially as the temperature decreases. The imaginary part of the impedance at point **b** increases much more than the real part, and this holds true for point **c**. Compared with  $20\text{ }^{\circ}\text{C}$ , the real and imaginary parts of the impedance of point **b** at  $-20\text{ }^{\circ}\text{C}$  increase to 14.15 and 28.56 times, respectively, and they increase to 16.06 and 30.25 times at point **c**, respectively.

The data from Tippmann et al. [67] show that the results obtained from EIS tests of batteries at different State of Charge (SOC) are also different; for example, at  $0\text{ }^{\circ}\text{C}$ , there is no change at point **a** for 100% SOC and 90% SOC, but both point **b** and point **c** are different. The real part of impedance 100% SOC at point **b** increases by 31.05%, and the imaginary part increases by 25.87% compared to those at 90% SOC, while at point **c** they increase by 36.67% and 101.74%, respectively.

#### 2.4. Degradation

During the actual operation of EVs, the power battery is likely to operate at subzero temperatures. Cycling the battery at low temperatures is likely to rapidly shorten the lifetime of the battery. More seriously, charging at low temperatures probably causes lithium deposition on the surface of the negative electrode to generate lithium dendrites, the growth of which may puncture the separator and trigger safety hazards such as internal short circuiting and thermal runaway of the battery.

The internal resistance of the battery increases when the battery is cycled at low temperatures. The increase of the internal resistance will not only have a negative impact on the battery performances (capacity reduction and power fade) but also on the energy efficiency of the battery [55]. Furthermore, the increased resistance leads to the increased temperature raise in the cells, leading to an inconsistent temperature distribution of the battery, which will further increase and accelerate the aging phenomena in the battery [56,70]. Zhang et al. [71] found that capacity and internal resistance exhibited highly similar changing behavior. After undergoing around 450 cycles, the capacity degradation apparently slows down, which is in sharp contrast with the rapid capacity degradation before 450 cycles. This point is considered to be the turning point in the low-temperature aging process of the batteries. In order to further clarify the mechanism of lithium plating evolution at low temperatures, they disassembled cells that had undergone different cycles to characterize the microstructure of the anode.

Then, they found that prior to the turning point, along with cycling, lithium plating happens quickly, and long lithium dendrites grow rapidly and interlace with each other, thus, rapidly covering the graphite surface, as illustrated in Figure 6. However, after the turning point, lithium plating happens sluggishly, and the anode surface morphology has little changed. That is similar to the change in capacity and internal resistance of batteries.

In addition, Ouyang et al. [7] have studied the effect of different aging conditions on battery capacity degradation. A cycle life test was performed at  $-10\text{ }^{\circ}\text{C}$  on 13 cells under varied charge current rates, charge cut-off voltages, and charge cut-off currents to analyze the aging mechanism when charging an LIB at a low temperature. They found that the cells degrade nonlinearly as the charging current rate and cut-off voltage increase (Figure 7). There exists a turning point in the capacity retention for both charging parameters, indicating a distinct degradation once the magnitude of the parameters exceeds a certain level.

They further investigated the effect of change in cut-off current on capacity decay and concluded that the decay starts at a constant current stage.

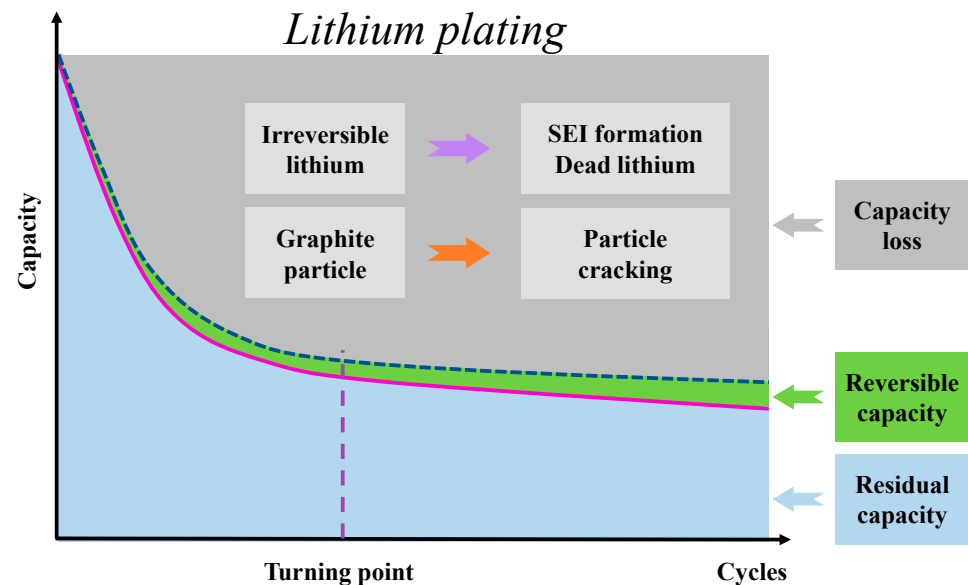


**Figure 6.** Schematic of battery degradation mechanisms during long-term low-temperature cycling [71].

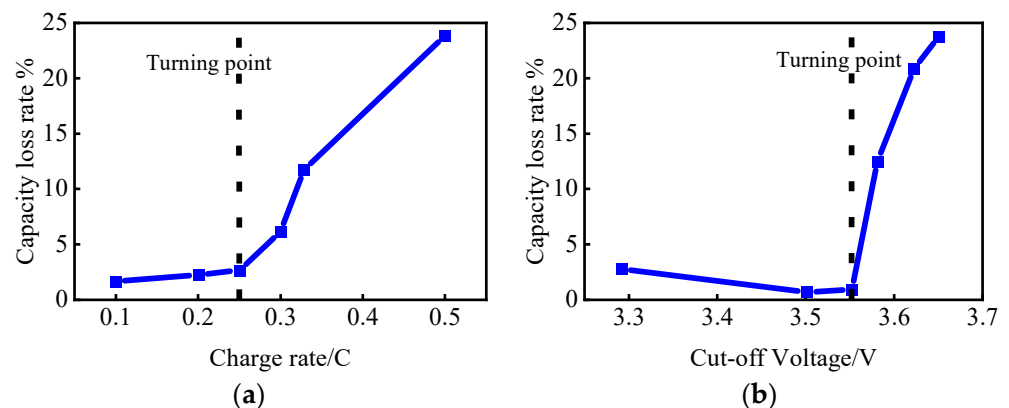


**Figure 7.** Turning points of capacity loss rate after 40 cycles for different charging parameters: (a) charging rate; (b) cut-off voltage of charging [7].

In order to provide a detailed understanding of the cycle degradation of LIBs at low temperatures, Table 8 lists the relevant literature, including cell capacity, cell type, cell material, experimental temperature and experimental multiplier, cycles at the 80% lifetime, aging rate (%/cycle), and aging rate in the first 100 cycles (%/cycle). From Figure 8, we can see that the normalized aging rate of the battery increases exponentially as the temperature decreases. The aging rate of large-capacity batteries is observed to vary slightly with temperature, while the variation is high for low-capacity batteries. For example, the aging rates for batteries of the same material (NCM) at  $-10\text{ }^{\circ}\text{C}$  are 1.1, 11.4, and 13.3 times higher than those at room temperature for the 37 Ah battery in the literature [71] and the 3 Ah and 1.5 Ah batteries in the literature [69], respectively. In addition, the aging rate of batteries at low temperatures is also related to the cycling conditions, which increase with the C-rate in an approximately linear way. For example, in the literature [66], the aging rate at  $-10\text{ }^{\circ}\text{C}$  for 1 C-rate cycling is 6.9 times higher than that for 0.2 C-rate cycling at the same temperature.

Table 8. Aging rate of LIBs at low temperatures.

Nominal Capacity (Ah)	Battery Type	Material	T (°C)	Cha. C-Rate	Disch. C-Rate	Cycles at the 80% Lifetime	Aging Rate (%/Cycle)	Aging Rate in the First 100 Cycles (%/Cycle)	Ref.	
2.500	Cylindrical 26650	LFP	−22	1 (100% DOD)	0.5	92	0.140	0.224	[72]	
				1 (80% DOD)		99	0.123	0.202		
				0.5 (80% DOD)		140	0.104	0.150		
3.100	18650	-	−10	0.2	0.5	-	0.049	0.060	[66]	
				1		-	0.049	0.059		
				0.2		-	0.102	0.113		
				1		135	0.147	0.153		
2.300	High-quality Cylindrical 26650	LFP	RT <sup>a</sup>	1	-	2594	0.008	-	[56]	
				1		2072	0.010	-		
				1		193	0.104	-		
				1		193	0.104	-		
37.000	Large format Prismatic	NCM	RT <sup>a</sup>	2	2	186	0.041	0.109	[71]	
				2		184	0.045	0.125		
1.500	High-power 18650	NCM + LMO	RT <sup>a</sup>	1	1	-	0.013 <sup>b</sup>	-	[73]	
				0		1	-	0.038 <sup>b</sup>		-
				−10		1	-	0.102 <sup>b</sup>		-
				−20		1	-	0.198 <sup>b</sup>		-
39.000	Large format Pouch bag	NCM	RT <sup>a</sup>	-	-	-	0.004	0.003	[74]	
				0		-	-	0.009		0.012
16.000	Pouch	NCM	RT <sup>a</sup>	1	-	-	0.004	-	[75]	
				2		-	0.008	-		
				1		-	0.012	-		
				2		-	0.018	-		
3.000	18650	NCM	RT <sup>a</sup>	1/3	1/3	-	0.043	0.080	[69]	
				10		1/3	-	0.157		0.100
				0		1/3	-	0.361		0.300
				−10		1/3	-	0.490		0.490
2.600	18650	NCA	RT <sup>a</sup>	1/3	1/3	-	0.010	0.030	[69]	
				10		1/3	-	0.017		0.050
				0		1/3	-	0.222		0.200
				−10		1/3	-	0.301		0.320
1.500	18650	NCM	RT <sup>a</sup>	1/3	1/3	-	0.003	0.000	[69]	
				10		1/3	-	0.013		0.000
				0		1/3	-	0.020		0.020
				−10		1/3	-	0.040		0.040
1.100	18650	LFP	RT <sup>a</sup>	1/3	1/3	-	0.007	0.000	[69]	
				10		1/3	-	0.007		0.000
				0		1/3	-	0.027		0.010
				−10		1/3	-	0.070		0.080
3.250	18650	NCA	RT <sup>a</sup>	0.5	0.5	290	0.062	-	[76]	
				0.5		3	2.672	-		
5.000	High-energy 21700	NCA + LNO	RT <sup>a</sup>	0.2	-	662	0.030	-	[57]	
				0.4		378	0.053	-		
				0.6		115	0.174	-		
				15		0.2	332	0.060		-
				0.4		117	0.171	-		
				0.6		54	0.370	-		
				0		0.2	18	1.111		-
				0.4		9	2.222	-		
−10	0.2	6	3.333	-						
	0.4	8	2.500	-						
11.500	Large format	LFP	−10	0.1	-	-	0.002	-	[7]	
				0.25		-	0.016	-		
				0.3		-	0.107	-		
				0.33		-	0.185	-		
				0.5		-	47	0.433		-

<sup>a</sup> 20~25 °C; <sup>b</sup> %/h. Depth of discharge (DOD).

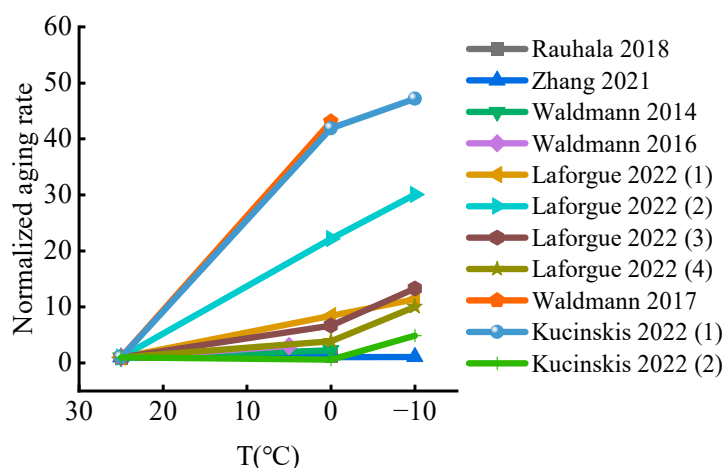


Figure 8. Normalized aging rate of batteries under different temperatures [56,57,69,71,73,75,76].

### 3. Low-Temperature Modeling

The mathematical model of LIBs is of great significance for battery state estimation and thermal management. Nonlinear behavior occurs in the battery, which is closely related to temperature. The commonly used models work well at room/elevated temperatures, but their accuracy decreases significantly at low temperatures. This can be explained by the fact that the behaviors of LIBs in low-temperature environments are affected by many factors: for example, the viscosity of the electrolyte increases at low temperature and the conductivity decreases; the film impedance and charge transfer impedance at the electrolyte/electrode interface increase; the migration rate of lithium ions in the active substance itself decreases, which makes the battery modeling more complex. In addition, considering the mutual coupling characteristics of the electrical and thermal behaviors of the battery in the low-temperature environment, the establishment of the electrothermal coupling model is essential to exactly describe the low-temperature characteristics of the battery.

#### 3.1. Equivalent Circuit Model (ECM)

The ECM is usually composed of open-circuit voltage (OCV), a single ohmic resistance, and a series of parallel resistance and capacitance (RC) networks [77], as shown in Figure 9a. The parameterization and simplicity of implementation make ECM the preferred choice for battery state estimation. The model parameters are usually obtained by Hybrid Pulse Power Characteristic (HPPC) test at different SOCs; however, the subzero temperature and high current rate will also affect the model parameters. The general ECM is difficult to describe the low-temperature characteristics of the battery, so it is often necessary to consider the influence of low temperature on the model parameters to improve the accuracy of the LIB model.

Considering some parameters in the ECM as temperature-dependent would increase the accuracy of models in describing the low-temperature characteristics, as shown in Figure 9b. Das et al. [78] considered the influence of low temperature on the parameters of LIB models and modified the commonly used ECM. By changing the resistance parameters in the RC network as a function of current rate, SOC, and temperature, the improved model is used to verify the ternary battery, which can accurately predict the battery terminal voltage behavior under low-temperature environments, as shown in Figure 10 and Table 9, where the low-temperature discharge curves of the traditional ECM and the improved ECM are compared.

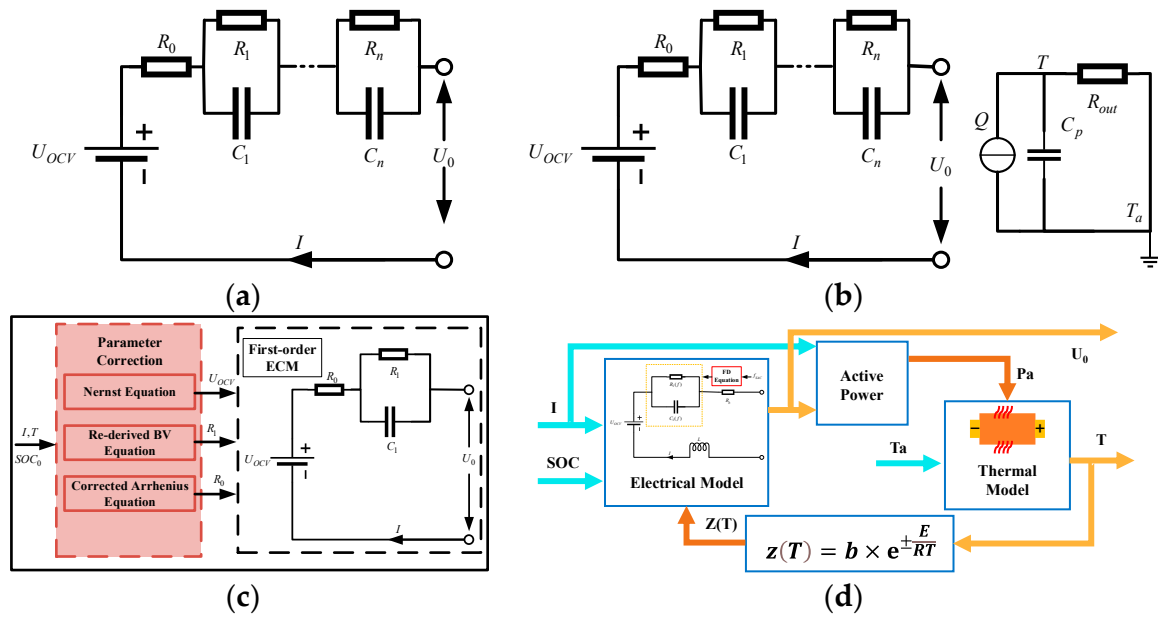


**Figure 9.** Representative ECM and its modified ones: (a) RC ECM [78]; (b) Electrothermal coupling model [79]; (c) Adaptive model 1 [80]; (d) Adaptive model 2 [81].

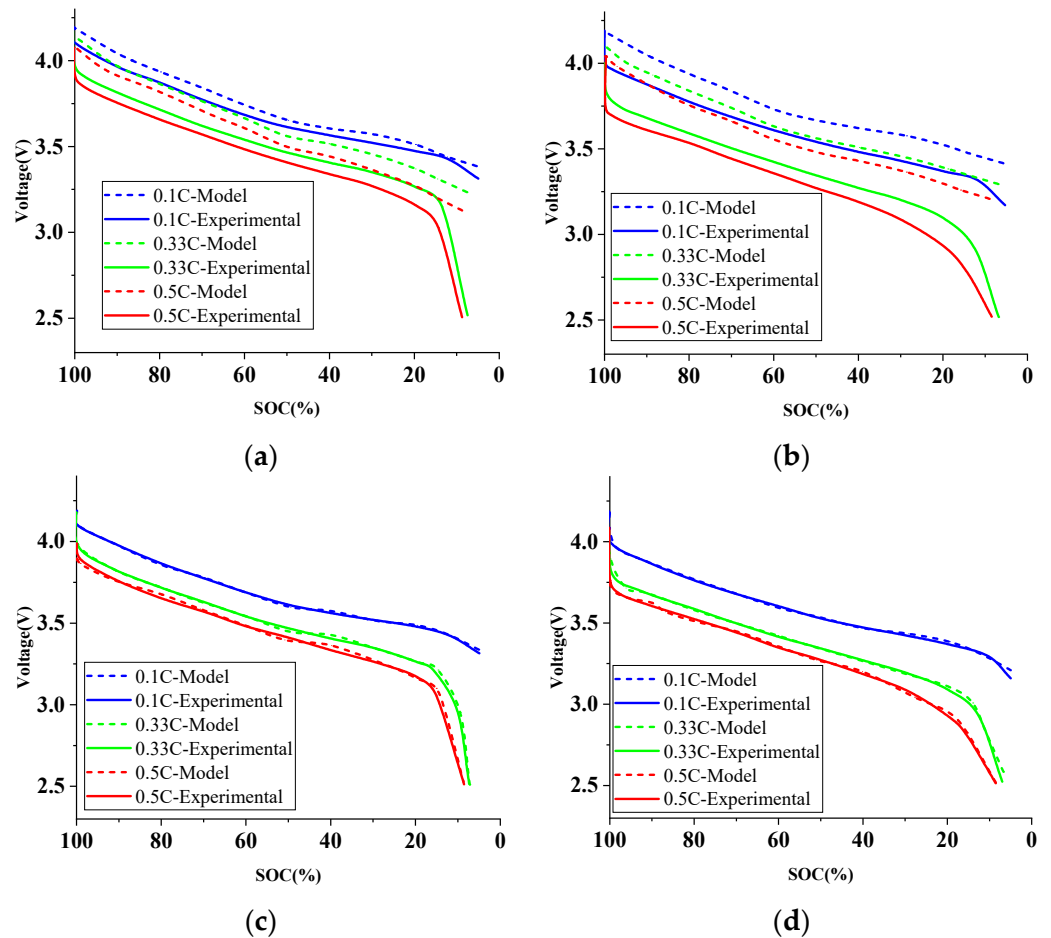


**Figure 10.** Validation of discharge curves at different C-rates using the traditional ECM at (a)  $-10\text{ }^{\circ}\text{C}$ , (b)  $-20\text{ }^{\circ}\text{C}$ ; Validation of discharge curves at different C-rates using the improved ECM at (c)  $-10\text{ }^{\circ}\text{C}$ , (d)  $-20\text{ }^{\circ}\text{C}$  [78].

**Table 9.** Summary of improved equivalent circuit model.

Material	Model	Parameterization Conditions	Modeling Considerations	Validation Conditions	Modeling Accuracy Evaluation			Ref.
NCM	Figure 9b	T SOC I −30~−10 °C 0~100% 0.1~0.5 C-rate	$R_1 = f(T, SOC, I)$	−30 °C, 0.1~0.5 C-rate	MPE 0.38~4.3%	APE 0.24~0.5%	[78]	
LTO	Figure 9c	T SOC I 5~45 °C 10~90% 1~4 C-rate	$U_{OCV}, R_0 = f(T)$ $R_1 = f(T, I)$	5 °C, 1 C-rate 5 °C FUDS Test	ME <sup>C</sup> 28.68 mV ME <sup>C</sup> 228.9 mV	ME <sup>P</sup> 4.45 mV ME <sup>P</sup> 81.7 mV	[80]	
NMC LCO LFP	Figure 9d	T f −15~−0.3 °C 50~5k Hz	$R_1(f), C_1(f) = f(T, f)$	−15~−10 °C, 50~5k Hz	MRE 1.68~2.12%	AE 13.6~26.7 mV	[81]	
NMC	Figure 9b	T SOC I −20~45 °C 10~100% 0.5~4 C-rate	$R_0, R_1, C_1 = f(T, SOC, I)$	−20 °C and −10 °C, 0.5~5 C-rate Disch.	RMSE < 0.1 V		[79]	
NMC	Figure 9b	T SOC −10~55 °C 0~100%	$U_{OCV}, R_0, R_1, C_1,$ $R_2, C_2 = f(T, SOC)$	−10 °C 0 °C 25 °C 45 °C	RMSE 3.98% 2.93% 2.66% 3.00%	MAEE 1.91% 1.27% 1.00% 0.80%	[82]	
LFP	Figure 9b	T SOC −20~25 °C 0~100%	$U_{OCV} = f(SOC)$ $R_0, R_1, C_1 = f(T, SOC)$	Under the real driving cycle conditions at −20 °C	AE < 3%		[63]	

<sup>C</sup> Conventional Model, <sup>P</sup> Proposed Model. Federal urban driving schedule (FUDS); Maximum percentage error (MPE); Average percentage error (APE); Maximum error (ME); Maximum relative error (MRE); Average error (AE); Root mean square error (RMSE); Maximum absolute estimation error (MAEE).

Zhu et al. [79] presented an improved electrothermal coupling model, which studied the dependence of all impedance parameters (resistance and capacitance) involved in the model on temperature, SOC, and current, and established the dependence through the Butler–Volmer equation, Arrhenius equation, and polynomial regression analysis. The validation results showed that the improved model can better predict the high-power operation scenario of the battery in the low-temperature environment.

Fang et al. [82] had established a second-order RC ECM with temperature compensation function to evaluate the impact of temperature change on the SOC estimation of ternary batteries. According to a dual-fifth polynomial, the two-dimensional mathematical expression relationship between all model parameters and temperature and SOC is established. The results show that the temperature has a great influence on the model parameters, especially in the low-temperature adaptability.

Jaguemont et al. [63] developed a first-order RC ECM coupled with a thermal model for a 100 Ah lithium–iron–phosphate ion battery. The parameters change with the SOC and temperature, and the parameters are obtained by the two-dimensional table lookup method. It is verified that the electrothermal coupling model can better simulate the temperature and voltage curves under constant current discharge conditions, as shown in Figure 11.

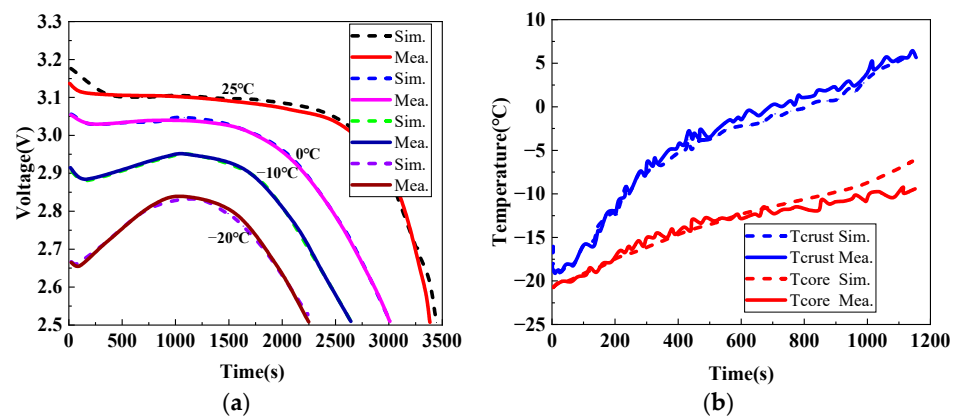


**Figure 11.** Verification of electrothermal coupling model: (a) 100 A discharge voltage curve at four sets of temperatures (−20 °C, −10 °C, 0 °C, and 25 °C); (b) Battery temperature core and crust for a 262 A discharging current and  $T_{test}$  of −20 °C [63].

Chen et al. [80] developed a different model by combining first-order ECM with electrochemical equations for a high-power LTO battery. The Butler–Volmer equation was simplified and embedded into the first-order RC ECM to characterize the polarization behavior of the battery at different current rates and temperatures. Furthermore, the Nernst equation and Arrhenius equation corrected by quadratic polynomial are considered to describe the effect of temperature on the OCV and ohmic internal resistance of the battery, respectively. The validation under constant current and dynamic conditions showed that the improved model is superior to the traditional ECM for the tested high-power batteries.

Jiang et al. [81] simplified the complex fifth-order ECM to a first-order low-temperature model for the high-frequency range. Based on the proposed frequency-dependent equation, the polarization resistance and polarization capacitance change with frequency, and the model complexity was reduced, and it can simulate the low-temperature behavior of the battery with a simple structure when considering thermal behaviors of batteries.

### 3.2. Electrochemical Model

The electrochemical model can simulate the physical and chemical phenomena inside the battery, which generally provides a relatively high accuracy. The P2D model proposed by Newman et al. [83] is a commonly used electrochemical model. The porous electrode theory and macroscopic homogeneous method are used to describe the change of the solid–liquid phase potential, and the concentrated solution theory and Fick diffusion law are used to describe the lithium-ion concentration in the solid and liquid phases. The single-particle (SP) model reduces the complexity of the model by simplifying the liquid-phase dynamics and using two spherical particles to represent the positive and negative electrodes of the LIB, respectively. The improved electrochemical model is summarized in Table 10.

Electrochemical models involve many parameters, and when establishing low-temperature electrochemical models, it is often necessary to consider temperature-sensitive parameters to adaptively change with temperatures for improving the accuracy of the model. Gholami et al. [84] studied the low-temperature electrochemical modeling of LIBs and conducted the sensitivity analysis of low-temperature parameters. They showed that negative electrode parameters have a much greater effect on battery performance at low temperatures than positive electrode parameters, and the effect of electrode porosity and the initial liquid lithium-ion concentration on the battery performance can be neglected. For example, at  $-30\text{ }^{\circ}\text{C}$ , the sensitivity of particle radius, active material volume fraction, and initial lithium-ion concentration in the negative electrode is about 49, 32, and 11 times higher than those in the positive electrode, respectively. Similarly, in the negative electrode, the sensitivity of particle radius is about 1.4 times and 2 times higher than that of the active material volume fraction and initial lithium-ion concentration, respectively.

Some studies have added a lumped thermal model to the P2D model and modified relevant equations or parameters to make it suitable for low-temperature scenarios, as shown in Figure 12c. Wang et al. [85] developed a simplified discrete electrochemistry–thermal coupling model suitable for low-temperature environments based on the P2D model by fitting the lithium-ion concentration in the form of parabola and simplifying the description of the solid–liquid diffusion control equation. The model with parameters updated with temperature can better simulate the “trough” phenomenon of multistage constant current discharge potential difference at low temperature ( $-20\text{ }^{\circ}\text{C}$ ). An et al. [86] considered the relationship between temperature-related parameters and low temperature, in which the diffusion coefficient and reaction rate constant were fitted by Arrhenius formula, and the lithium-ion diffusion rate, conductivity, and thermodynamic factor were fitted by polynomial, and thus proposed an electrochemical–thermal coupling model. The modeling results showed that the concentration gradient of lithium ion in liquid and solid phases is greatly affected by the temperature, especially at low temperatures. Xu et al. [87] proposed a prismatic LIB electrochemical–thermal coupling model. After dividing the temperature

range into several intervals, the model parameters were calibrated separately to verify from a wide temperature range ( $-5\sim 55\text{ }^{\circ}\text{C}$ ), and the model accuracy was high.

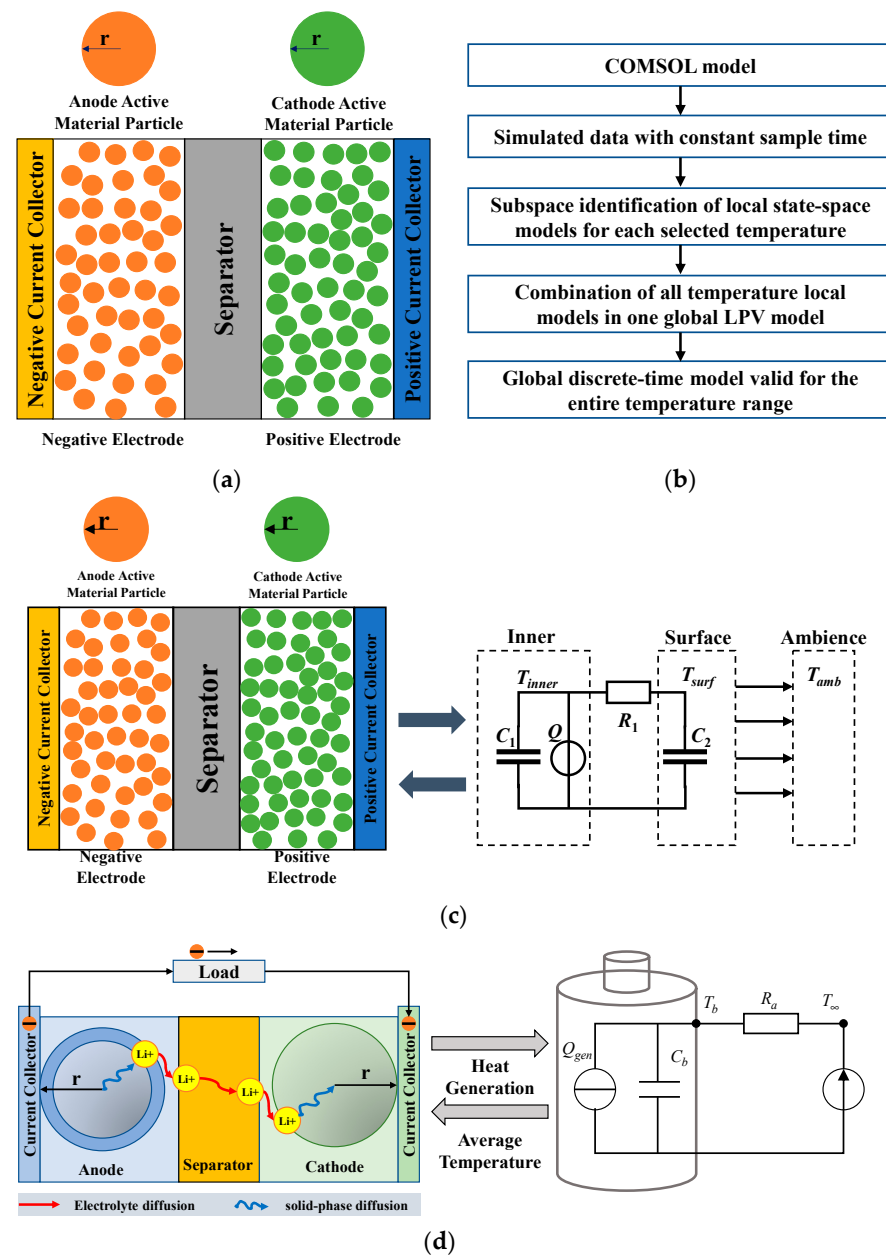


**Figure 12.** Representative electrochemical model and its modified ones: (a) P2D model [84]; (b) Overall schedule of the model reduction process using system identification [88]; (c) Electrochemical-thermal coupling model [85]; (d) Simplified electrochemical-thermal coupling model [89].

Li et al. [89] developed a simplified electrochemical model with variable solid-phase diffusion (particularly considering concentration dependence on temperature) using model simplification techniques such as single-particle hypothesis and polynomial approximation, as shown in Figure 12d. By analyzing the internal dynamics of the battery, all parameters were classified, and parameter identification in a wide temperature range ( $-20\sim 45\text{ }^{\circ}\text{C}$ ) was studied. The results showed that, especially under low-temperature conditions, the voltage and temperature predictions of the proposed model were better than those of the constant solid-phase diffusion model, as shown in Figure 13.

**Table 10.** Summary of improved electrochemical model.

Material	Model	Parameterization Conditions	Modeling Considerations	Validation Conditions	Modeling Accuracy Evaluation		Ref.
LCO	Figure 12c	T −20~40 °C	$P_{s,n}^{dyn}, P_{s,p}^{dyn}, P_{e,n}^{dyn}, P_{e,n}^{ste}, P_{e,p}^{dyn}, P_{e,p}^{ste}, P_{act,n}, P_{act,p}, R_{ohm,e}, R_{ohm,s}, R_{SEI}, U_{OCV} = f(T)$	−20~0 °C, 0.3 C-rate	ME 25.8~72.9 mV	SD <sup>b</sup> 7.79~15.1 mV	[85]
LCO <sup>a</sup> LNO NCM NCO LMO	Figure 12c	T <−30 °C	Electrolyte conductivity is considered as a function of temperature and concentration.	LCO −40 °C LNO −40 °C NCM −40 °C NCO −40 °C LMO −30 °C	RMSE	150 mV 110 mV 100 mV 130 mV 90 mV	[84]
LFP	Figure 12c	T 0~55 °C	$D_2, v, \sigma_2 = f(T, C)$ $k_{0,i}, U_{OCV} = f(T)$	The modeling results show that the lithium-ion concentration gradient in liquid and solid phases is greatly affected by temperature, especially at low temperatures.			[86]
LCO	Figure 12d	T −20~45 °C	$D_{s,i} = f(C)$ $D_{s,n}, D_{s,p}, \tau_e,$ $K_n, K_p, U_{OCV} = f(T)$	−20~25 °C	MAE 37.8~59.3 mV	RMSE 39.9~79.2 mV	[89]
NMC	Figure 12b	T I −25~40 °C 0.1~6 C-rate	$D_{a,n}, k_{an}, k_{cat},$ $D_1, v_1, \kappa_1, U_{OCV} = f(T)$	15 °C	RMSE 15 mV	ME 40 mV	[67]
NMC	Figure 12c	T −5~55 °C	$P_{comp}, \tau_e, R_{ohm}, \tau_n = f(T)$	−5~55 °C	MAE 19.68~26.56 mV	MAE 0.0433~0.0745 °C	[87]
NMC	Figure 12b	T I −25~40 °C 0.1~6 C-rate	$D_{a,n}, k_{an}, k_{cat},$ $D_1, v_1, \kappa_1, U_{OCV} = f(T)$	0 °C	MAE <sup>c</sup> 2.9 mV		[88]

<sup>a</sup> LiNi<sub>0.8</sub>Co<sub>0.2</sub>O<sub>2</sub> (NCO); <sup>b</sup> Standard deviation (SD); <sup>c</sup> Mean absolute errors (MAE).

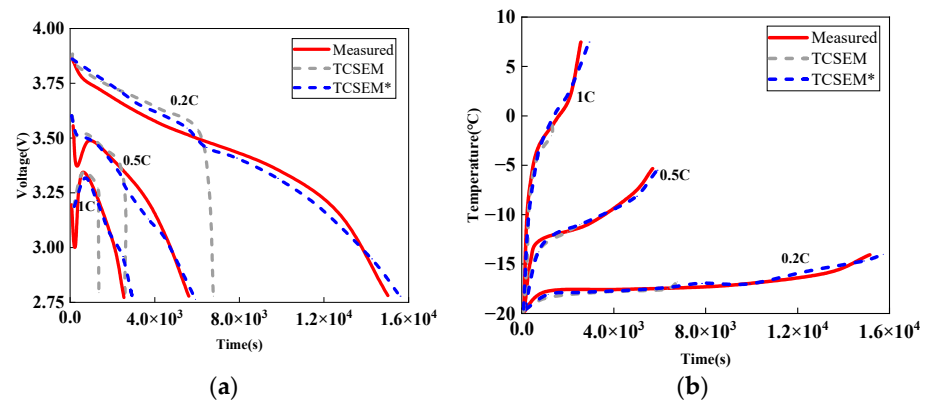


**Figure 13.** Voltage and temperature response under constant current discharge test at −20 °C: (a) Voltage; (b) Temperature [89]. Model with constant solid-phase diffusion (TCSEM) and model with variable solid-phase diffusion (TCSEM\*).

Tippmann et al. [67] proposed a fully parameterized electrochemical model, as shown in Figure 12b. The temperature-dependent parameters in the model were studied using EIS data and verified through constant current discharge conditions. The proposed model was suitable for low-temperature (−25 °C) and high-magnification (6 C-rate) conditions. Based on this work, Remmlinger et al. [88] proposed a simplified electrochemical model based on the system identification method, which can predict terminal voltage and anode potential. The discrete time linear parameter change model was used as the model form, which can better simulate the nonlinear behavior of LIBs and accelerate the calculation speed.

### 3.3. Aging Model

Table 11 presents the aging models developed especially for battery applications at low temperatures, where the changes from the room-temperature model are highlighted. Liu et al. [90] quantitatively analyzed the degradation reasons of LIBs from the aspects of capacity, incremental capacity (IC), differential voltage (DV), and EIS. The results showed that the loss of active materials and lithium plating were the main reasons for the low-temperature degradation of batteries. In addition, the loss of conductivity was three times higher at low temperatures than that at room temperature. The quantized results were considered as the input of the convolutional neural network and long short-term memory

(CNN-LSTM) prediction model, which can accurately forecast the capacity aging of LIBs in the low-temperature environment (Figure 14a).

**Table 11.** Summary of aging model.

Material	Working Condition		Change	Contrast Accuracy		Ref.
	T	I				
NMC	-15~25 °C	-	$Q = f(c, IC, DV, EIS)$	AE	<5%	[90]
NMC	-20~0 °C	0.2~1 C-rate	$Q_T = f(T); Q_I = f(I);$ $Q_U = f(U); Q_{T \times I} = f(T, I);$ $Q_{T \times U} = f(T, U);$ $Q_{(T \times U) \times (T \times I)} = f(T, U, I)$	ME	<10%	[91]
LFP	-20~25 °C	-	$Q_{ca} = f(T, t)$ $Q_{cy} = f(T, t)$ $Z_{in} = f(T, N, t)$	AE <sup>CA</sup> AE <sup>CY</sup> AE <sup>R</sup>	2.3% 3.2% 8.5%	[92]
NMC	-5 °C	1/6 C-rate 1/3 C-rate 2/3 C-rate 1 C-rate 2 C-rate	$Q = f(I)$	AE <sup>CL</sup> AE <sup>CL</sup> AE <sup>CL</sup> AE <sup>CL</sup> AE <sup>CL</sup>	0.064% 0.324% 0.149% 0.472% 1.605%	[54]

<sup>CA</sup> Calendar aging, <sup>CY</sup> Cycle aging, <sup>R</sup> Resistance increment, <sup>CL</sup> Capacity loss.

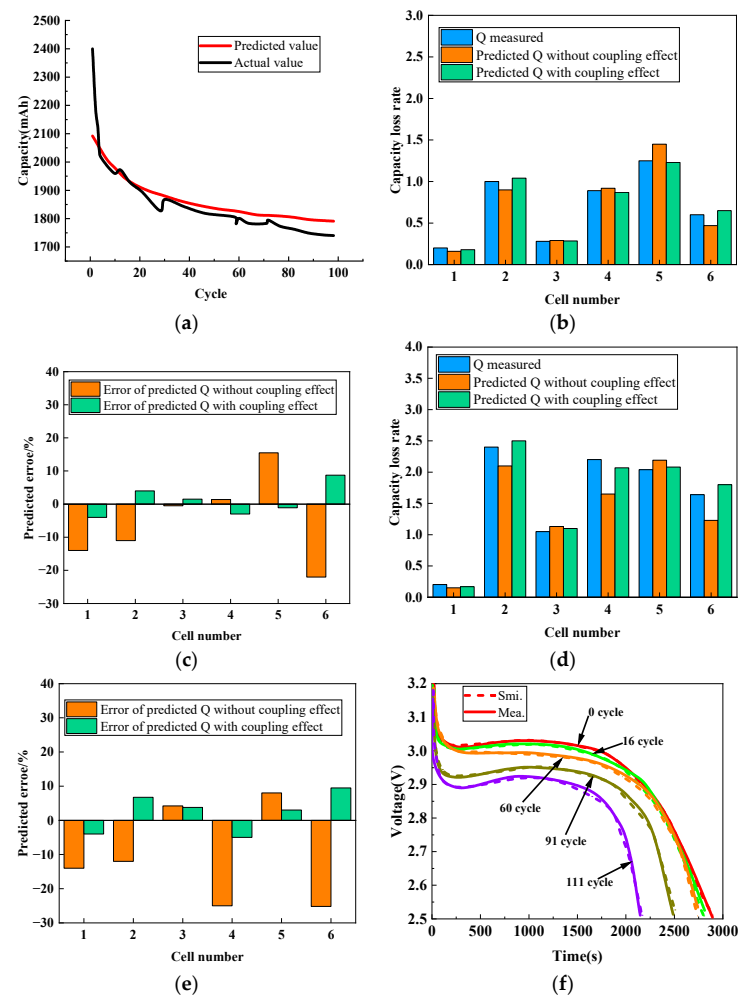
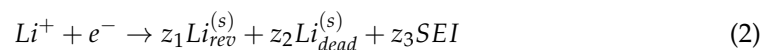


**Figure 14.** Actual and predicted results: (a) CNN-LSTM prediction model [90]. The predicted capacity loss rate and prediction error in 1st-phase and 2nd phase: (b) Predicted and measured k in 1st phase; (c) Prediction error in 1st phase; (d) Predicted and measured k in 2nd phase; (e) Prediction error in 2nd phase [91]. (f) Evolution of the capacity as the cell ages for the cycle aging test at 0 °C [92].

You et al. [91] defined capacity degradation at 0~10% as the 1st phase of aging, and capacity degradation at 10~20% as the 2nd phase of aging. Based on the orthogonal experimental results, the influence of charging rate, charging temperature, and charging cut-off voltage on battery aging was considered. Among them, the temperature in the first stage had the greatest impact on battery aging, and the charging cut-off voltage in the second stage increased the capacity degradation. The coupling effect between different factors was analyzed by means of distance analysis and variance analysis, and a low-temperature capacity decline model with multiple factors was established. The experimental results showed that the capacity decay model considering coupling effect had good accuracy at low temperature.

Jaguemont et al. [92] developed an aging model based on the research on the aging of LIBs at subzero temperatures. He identified the following factors for low-temperature battery decline: loss of cyclable lithium, loss of electrode active materials, and decrease in accessible surface area (equals an impedance rise). Calendar aging mainly took time and temperature into account and used a quartic polynomial for fitting regression; cycling aging took the number of cycles and temperature as the fitting parameters, and used the MATLAB curve-fitting tool to complete the fitting. The impedance increment consisted of two parameters, including cyclic aging test impedance and calendar aging impedance.

For LIBs with graphite as the negative electrode, lithium plating will cause serious deterioration of the battery. Ren et al. [54] established an electrochemical model of lithium plating and stripping reactions by studying lithium plating and stripping reactions at low temperatures, thereby achieving quantitative detection of lithium plating. According to the reaction of the anode, the low-temperature charging and subsequent rest process were divided into four stages, as shown in Figure 15. The results showed that this method can predict the characteristic voltage platform during the rest period after low-temperature charging, and can simulate the capacity loss caused by lithium plating reaction at different magnification.



$$j = j_1 + j_2 + j_3 \quad (4)$$

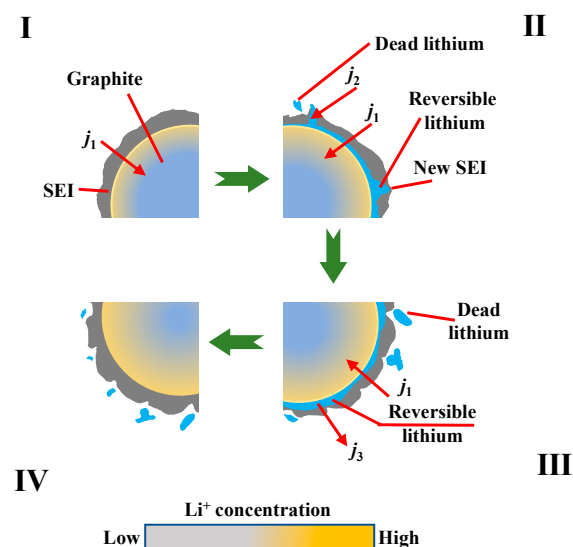


Figure 15. Illustration of the lithium plating–stripping process [54].

#### 4. Low-Temperature Heating

Because the performance decrease of LIBs in low-temperature environments is recoverable, the performance of LIBs will be restored to the level under normal temperature if the operating temperature of LIBs is raised using the techniques, such as low-temperature heating approaches. The low-temperature heating technology of LIBs has good adaptability, which can meet the use of power battery under low-temperature conditions, and is also the mainstream solution to solve the poor low-temperature performance of LIBs at present. According to the different modes of heat transfer and generation in the heating process, the low-temperature heating of LIBs can be generally divided into internal heating, external heating, and hybrid heating, as shown in Figure 16. According to whether the heat is generated by the internal resistance of the battery itself or by an external heat element, the heating method can be categorized into internal heating [93–99] and external heating [100–102]. Hybrid heating is a heating method that includes internal and external heating [103–106]. The most special is the self-heating lithium-ion battery [107,108], the battery internal embedded nickel foil to realize the heating of the battery. On the one hand, the nickel foil is a part of the battery in terms of physical structure, which is the “internal resistance” of the battery and can be seen as internal heating; on the other hand, the nickel foil is an external component of the battery in terms of electrochemical reaction, which is not the internal resistance of the battery and can be regarded as hybrid heating.

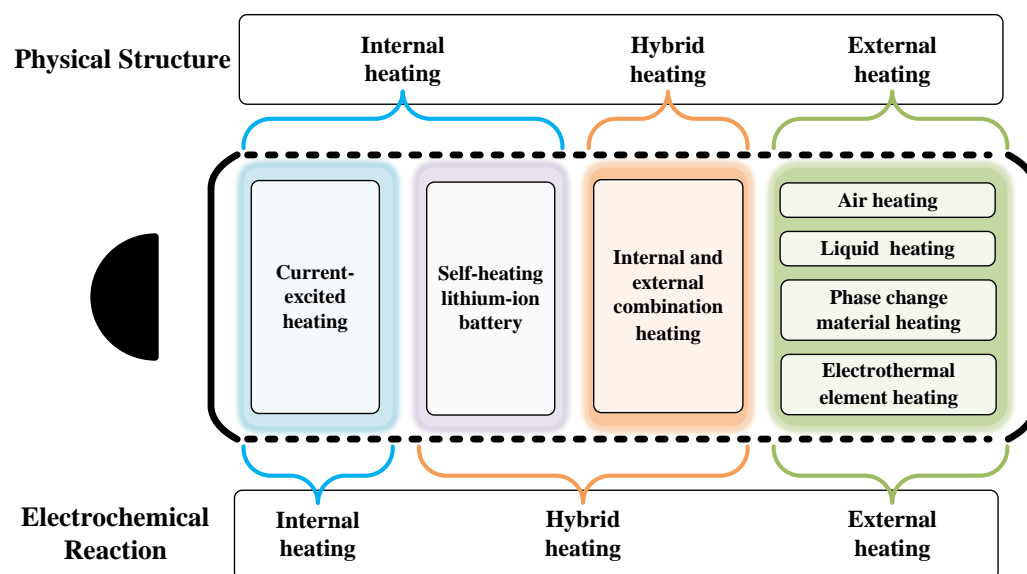


Figure 16. Classification of low-temperature heating for LIBs.

##### 4.1. Internal Heating

Classified from the perspective of physical structure, internal heating includes current-excited heating and SHLB technology; current-excited heating is categorized according to different current excitations applied to the battery, including direct current (DC) heating, AC heating, and AC–DC-superimposed heating.

##### 4.1.1. Current-Excited Heating

Constant-current discharge (CCD) heating means that the current remains constant during the heating process. Wu et al. [93] studied the relationship between discharge rate, heating time, and power consumption under constant-current discharge condition based on the battery temperature rise model and the ampere-hour integral. The results show that when the discharge rate is 2 C-rate, the heating rate is 3.21 °C/min, and the power consumption does not exceed 15% of the rated capacity; when the discharge rate is 1 C-rate, the heating rate is 0.83 °C/min, and the power consumption is almost 30% of the

rated capacity; when the discharge rate is less than 1 C-rate, the heating time and power consumption are significantly increased.

Constant-voltage discharge (CVD) heating means that the voltage remains constant during the heating process. Ji et al. [94] studied the effect of constant-voltage discharge on the low-temperature heating of the battery. For constant-voltage discharge mode, the lower the voltage, the shorter the heating time. The heating rate corresponding to 2.8 V discharge voltage can reach 6.6 °C/min.

Ruan et al. [95] proposed an optimized heating strategy based on discharge voltage, aiming at minimizing both heating time and capacity decay. The capacity loss is obtained by establishing the attenuation model, and the Pareto front of heating time and capacity loss is obtained by genetic algorithm. After normalization, the influence of weight coefficient on heating effect is discussed, and the optimal heating strategy is obtained. The experimental results showed that lower discharge cut-off voltage will shorten the heating time but will increase the capacity decline. The optimal heating voltage is 2.43 V. In order to achieve the constant discharge cut-off voltage during the heating process, the trapezoidal current method is used to ensure the constant voltage. This heating method can raise the battery from −30 °C to 2.1 °C in 103 s, and the average temperature rise rate can reach 18.7 °C/min. After 500 cycles of heating, the battery capacity loss is 1.4%, indicating that this heating method has little impact on capacity loss and greatly improves the low-temperature performance of the battery. This heating method comprehensively considers the impact of the discharge cut-off voltage on the heating time and capacity decline, but the energy of the battery during the discharge process is not fully utilized. Therefore, how to maximize the energy efficiency for the battery low-temperature preheating is a future research direction.

When the current excitation is AC, the SOC of the battery is kept unchanged, and the commonly used AC is a sinusoidal one. Zhang et al. [96] established a frequency domain heating model based on the equivalent circuit and studied the influence of the amplitude and frequency of the constant sinusoidal current (CSC) on the low-temperature heating method of the battery. Taking the 18650 batteries as an example, the battery temperature rises from −15 °C to 5 °C. When the AC amplitude is 7 A (2.25 C-rate) and the frequency is set to 1 Hz, the temperature rise rate of the battery can reach 2.33 °C/min, and the internal temperature uniformity of the battery is good. After repeated AC preheating tests, the battery capacity decline is experimentally validated as low. According to the preheating test results, when the AC frequency is constant, the heating time decreases with the increasing AC amplitude; when the AC amplitude is constant, the heating time increases with the increase of AC frequency. Besides the consideration of heating performance when selecting AC parameters, the possibility of lithium deposition also needs to be heeded.

Ruan et al. [97] proposed the optimal frequency heating strategy based on constant polarization voltage (CPV), taking into account the factors of heating time and life decay, based on the electrochemistry–thermal coupling model. The optimal heating frequency is deduced for maximum heat generation. The battery was heated from −15.4 °C to 5.6 °C in 338 s, with an average heating rate of 3.73 °C/min, and the temperature distribution is basically uniform. The experimental results show that the heating method has little effect on the battery life.

Jiang et al. [98] proposed a low-temperature heating strategy of AC plus DC. Through analysis and derivation, the expression of DC and AC amplitude ratio to prevent lithium deposition is obtained. The battery heating is realized by generating AC-superimposed DC current waveform through the soft-switch resonant circuit (Figure 17b). This method takes the battery itself as the heat source. By periodically controlling the MOSFET switch, the current passing through the battery can be AC-superimposed DC. By controlling the parameters such as capacitance and inductance, the ratio of DC to AC amplitude can be adjusted to reduce the risk of lithium plating in the battery. Through this circuit, the battery can be raised from −20.8 °C to 2.1 °C in 600 s, and the temperature difference between battery packs is less than 1.6 °C, which means that the heating method can achieve the

goal of uniform temperature distribution of LIBs. After 600 cycles of heating, no obvious aging characteristics of the battery were found, indicating that the heating method has a low impact on the battery life.

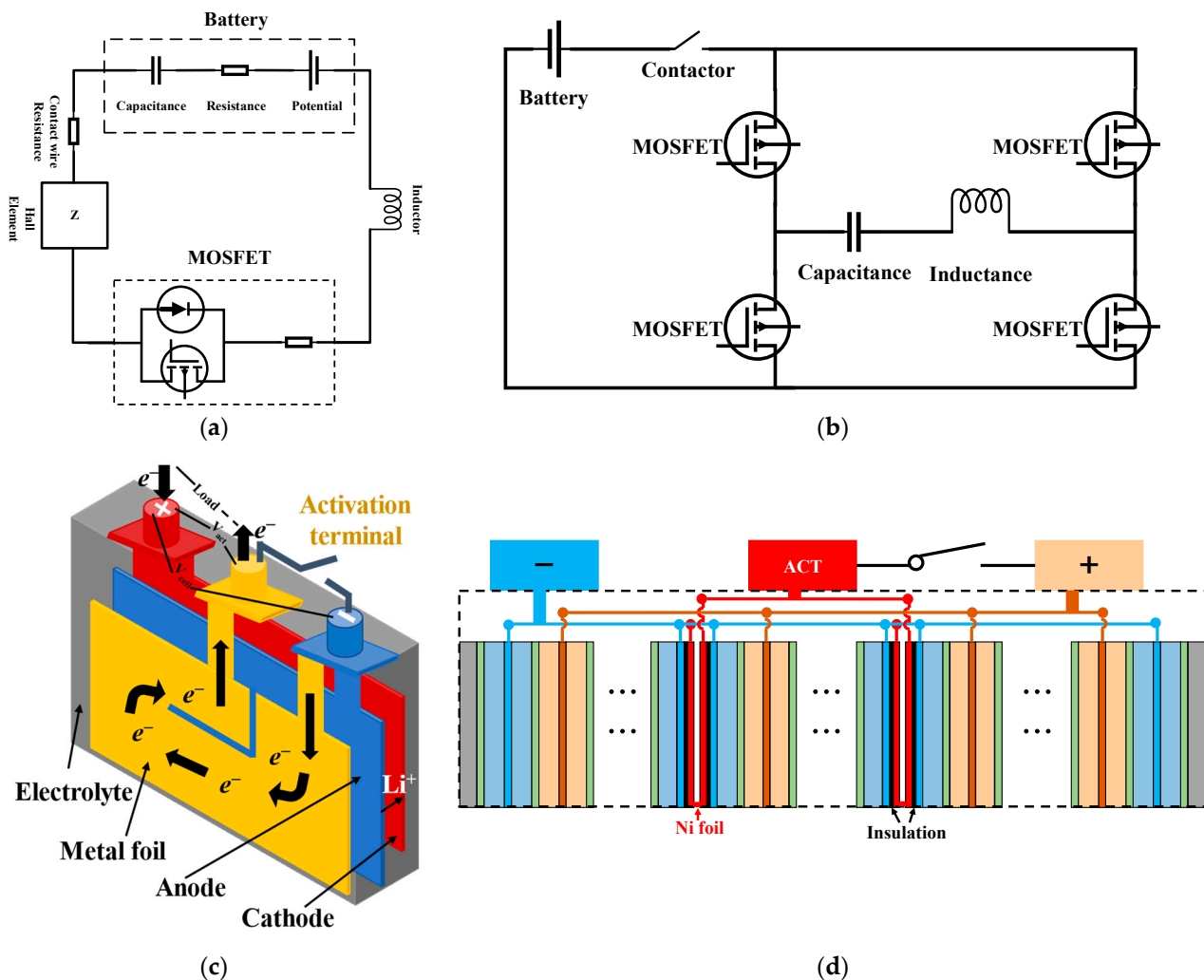


**Figure 17.** Internal heating technologies: (a) Pulse heating circuit [99]; (b) Soft-switching resonant circuit [98]; (c) SHLB heating structure diagram [107]; (d) SHLB with multiple nickel foils inserted [108].

Qu et al. [99] used MOSFET as the switch control element to realize pulse heating by designing the circuit, with the control circuit as shown in Figure 17a. The effects of switching frequency (0.1 Hz, 0.5 Hz, 1 Hz), different initial temperature, and SOC on heating were studied. The results showed that the switching frequency has little effect on heating rate, while the ambient temperature and initial SOC of battery have a significant effect on heating rate, and the heating rate can reach 6.86 °C/min.

#### 4.1.2. SHLB Heating

Wang et al. [107] achieved self-heating inside the battery by embedding nickel foil inside the battery, as shown in Figure 17c. The nickel foil leads out two tabs, one connected to the negative terminal and the other extended to the outside of the battery to form the active terminal. When the switch is closed, the current will generate a large amount of heat through the nickel foil, which will increase the battery temperature. When the battery temperature reaches the threshold, the switch is disconnected, and the battery stops self-heating and returns to the normal mode. The temperature-rise rate of this method can reach 60 °C/min. Yang et al. [108] compared the external heating method using a resistance heater with SHLB heating method and showed that the heating rate of SHLB is increased

by nearly 40 times. The more nickel foils embedded in the battery, the higher the heat production of the battery, the faster the temperature rise of the battery, and the better the temperature uniformity of the battery (Figure 17d).

It can be seen that the heating rate of the battery internal heating method is fast, and the temperature uniformity of the battery is good. However, DC self-heating would waste a certain amount of power, indicating low heating efficiency; AC self-heating battery power remains unchanged, but the need for an AC generator would increase the complexity of the heating circuit, and heating at high SOC poses a high risk of lithium plating; AC and DC superposition of the method avoids the risk of lithium plating, but it also reduces the heating rate, and requires additional design of circuits, increasing the complexity of the system. Compared with the traditional heating method, SHLB can achieve the purpose of rapid and efficient heating of the battery. However, because the heating scheme needs to change the internal structure of the battery, it is a huge uncertainty around the safety of the battery. At the same time, in order to reduce the temperature difference, it is necessary to embed multiple nickel sheets inside the battery, which increases the manufacturing difficulty and cost of the battery.

#### 4.2. External Heating

External heating mainly uses external heat sources to raise the temperature of the battery through convection or conduction heat transfer. It can be classified according to different external heat transfer methods, mainly including air heating, liquid heating, phase-change material (PCM) heating, and electric heating element heating. The efficiency of external heating is generally low, and the heating rate is slow.

Ji et al. [94] proposed an air-heating method and studied the influence of different heating resistance on heating efficiency and heating time (Figure 18a). If the selected heating resistance is smaller, the heating time is shorter and the heating efficiency is higher. When the battery is raised from  $-20\text{ }^{\circ}\text{C}$  to  $20\text{ }^{\circ}\text{C}$ , the heating resistance of  $0.4\ \Omega$  is selected, and the temperature-rise rate can reach  $28.24\text{ }^{\circ}\text{C}/\text{min}$ . It can be seen that the speed of temperature rise has increased significantly, but the internal temperature gradient of the battery is large, the fan increases additional costs, and the system construction is relatively complex, taking up a large space, which is not reasonable for the current lightweight requirements of EVs.

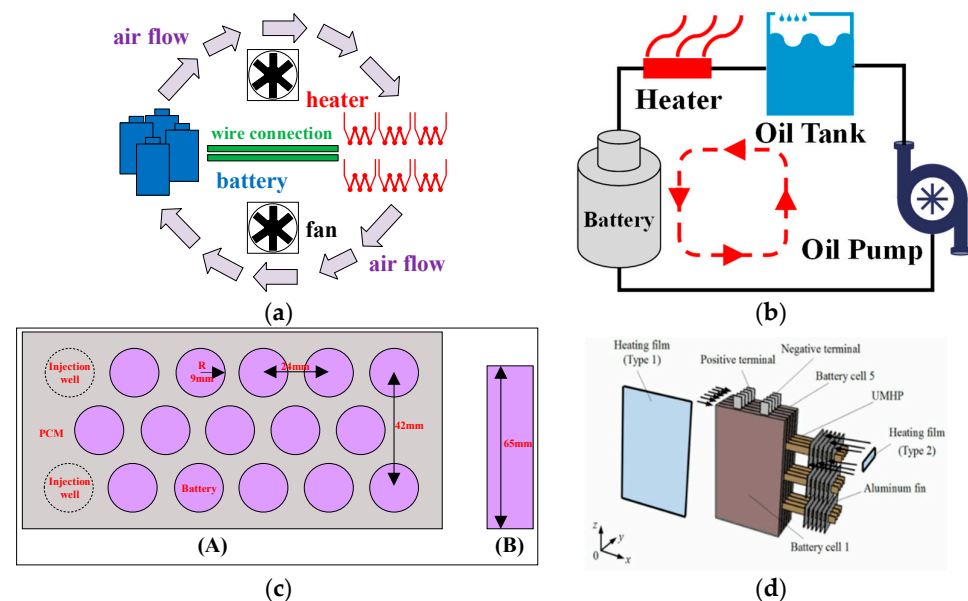


**Figure 18.** External heating technology: (a) Air heating; [94] (b) Liquid heating [100]; (c) PCM heating: (A) Top view of battery module; (B) Front view of battery module [101]; (d) Two heating methods: Type 1: directly attach the heating film to the maximum surface of the battery; Type 2: use ultra-thin micro-heat pipe (UMHP) for heating [102].

Wang et al. [100] evaluated the performance of the immersion preheating system by developing a three-dimensional Computational Fluid Dynamics (CFD) model (Figure 18b). Silicon oil is used as the heat-transfer fluid. Based on the simulation model, it is found that the heating rate is as high as  $4.18\text{ }^{\circ}\text{C}/\text{min}$ , and the temperature difference of the battery pack is less than  $4\text{ }^{\circ}\text{C}$ . However, the design of liquid heating systems is often complex, and costly, and requires good sealing performance, which is a huge challenge for practical engineering applications.

He et al. [101] proposed a PCM-based coupled heating rate measurement system with two hot plates at low temperatures for battery modules (Figure 18c). This strategy allows for a more uniform temperature distribution in the battery module.

Liu et al. [102] used the heating film and UMHP method to heat the battery at low temperatures and compared the heating effects of the two heating methods. The schematic diagram is shown in Figure 18d. Due to the long heat transfer path, the UMHP heating has a hysteresis. The reason is that the heat is transferred through UMHP, and the transfer path is long. When the ambient temperature was  $-20\text{ }^{\circ}\text{C}$ , the battery was heated by the heating-film method and the UMHP method, and the heating rate was  $6\text{ }^{\circ}\text{C}/\text{min}$  and  $4.8\text{ }^{\circ}\text{C}/\text{min}$ , respectively.

The external heating method is simple in principle and easy to implement, but there are obvious drawbacks such as large heating distance, slow heating speed, high energy consumption, and poor temperature uniformity.

#### 4.3. Hybrid Heating

Hybrid heating is a heating method combining internal battery heating and external battery heating, which can improve the heating rate and efficiency of the battery and reduce the temperature gradient of the battery.

Ruan et al. [103] proposed a compound heating method based on DC internal heating and external contact heating, which utilizes the battery's own discharge energy without additional power supply (Figure 19a). A distributed ECM is established to simulate the temperature change during low-temperature heating. Three conflicting targets, heating time, capacity loss, and temperature gradient, are considered and optimized by genetic algorithm. After normalization, the optimal heating strategy is obtained by analyzing the different weights. This heating method can raise the battery from  $-30\text{ }^{\circ}\text{C}$  to  $2\text{ }^{\circ}\text{C}$  within 62.1 s, and the average temperature rise rate can reach  $31\text{ }^{\circ}\text{C}/\text{min}$ . The low-temperature heating speed of the battery is very high, which reduces the heating energy consumption and reduces the battery life decline.

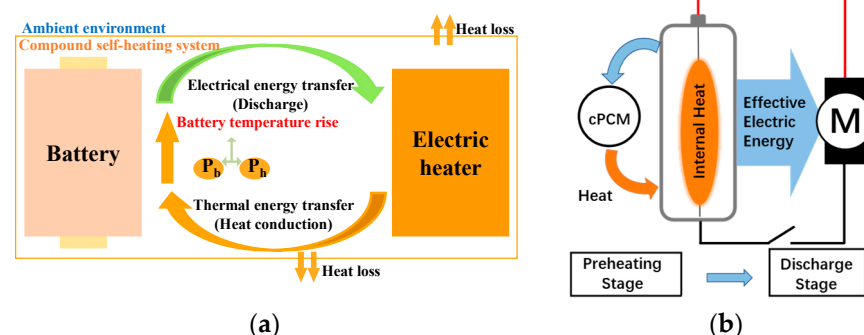


**Figure 19.** Schematic diagram of low-temperature hybrid heating: (a) Based on the inner-battery DC heating and outer-battery electric heating [103]; (b) Based on conductive composite phase-change materials (cPCM) [104].

Luo et al. [104] proposed a low-temperature battery pack preheating technique based on conductive cPCM, and the system can achieve a temperature rise rate of  $17.14\text{ }^{\circ}\text{C}/\text{min}$  and a temperature gradient of  $3.58\text{ }^{\circ}\text{C}$  (Figure 19b). An energy conversion model is devel-

oped to explain the energy conversion relationship of the battery under low-temperature heating to obtain the optimal heating strategy.

Xu et al. [105] proposed a battery low-temperature hybrid heating method in order to fully utilize the heat generated by the battery and the heating circuit. The battery and MOSFET are used as heat sources with a temperature rise rate of 11.22 °C/min, which shortens the heating time and reduces the energy consumption of the heating process.

Ruan et al. [106] developed a composite heating system including two externally heated aluminum sheets, which helps to fully utilize the discharge energy of the externally heated sheets. The basic electrical and thermal modeling of the heating system is performed and experimentally verified. Four key but conflicting heating metrics—heating time, heating efficiency, cell degradation, and temperature uniformity—are used to optimize the resistance of the external heater with an adaptive particle swarm optimization algorithm.

Compared with other heating methods, as shown in Table 12, hybrid heating methods feature a higher heating rate, and at the same time, they generally show less impact on the life of LIBs. Furthermore, the engineering realization for the hybrid methods is often easier, which is a more promising method of low-temperature heating for LIBs.

**Table 12.** Summary of low-temperature heating.

Heating Techniques	Battery Type	Temperature Range (°C)	Rate of Temperature Rise (°C/min)	Capacity Used	Other Key Parameters	Ref.
CCD heating	NCA 18650 2.60 Ah	−10.0~5.0	3.21 (2 C-rate)	15.0%	-	[93]
		−10.0~5.0	0.83 (1 C-rate)	30.0%		
CVD heating	NCM 18650 2.20 Ah	−20.0~20.0	5.00 (2 C-rate)	23.3%	-	[94]
			10.00 (3 C-rate)	20.0%		
			17.50 (4 C-rate)	15.1%		
CVD heating	NCM 18650 2.20 Ah	−20.0~20.0	6.70 (2.8 V)	23.0%	-	[94]
			12.00 (2.5 V)	17.5%		
	NCM Laminated 8.00 Ah	−30.0~2.1	18.70 (2.43 V)	20.0%	Capacity fade 1.40% (500 cycle) 4.95% (2000 cycle)	[95]
AC heating	NCA 18650 2.80 Ah	−20.0~5.0	1.67	-	-	[96]
			30.00 (1000 Hz)	-		
	NCM 18650 2.20 Ah	−20.0~20.0	14.10 (60 Hz) 8.80 (1 Hz) 8.60 (0.1 Hz) 7.10 (0.01 Hz)	-	-	[94]
CPV heating	NCM 18650 2.75 Ah	−15.4~5.6	3.73	-	-	[97]
AC + DC heating	NCM Laminated 35.00 Ah 12 cells pack	−20.8~2.1	2.29	6.6%	Temperature gradient <1.60 °C Capacity fade 0.43% (600 cycle)	[98]
Pulse heating	LCO 18650 2.00 Ah	−10.0~10.0	6.74	-	Capacity fade 20.00% (180 cycle)	[99]
Mutual pulse heating	NCM 18650 2.20 Ah	−20.0~20.0	11.66 (2.8 V) 19.90 (2.5 V) 29.82 (2.2 V)	4.9% 5.2% 5.1%	-	[94]
SHLB heating	NCM ACB <sup>a</sup> cell 7.50 Ah	−20.0~0.0	60.00 (single)	3.8%	Added weight 1.50% Added cost 0.04% Capacity fade 7.20% (500 cycle)	[107]
		−30.0~0.0	60.00 (single)	5.5%		
Air heating	NCM 18650 2.20 Ah	−20.0~20.0	11.94 (0.8 Ω 3.34 V)	7.5%	-	[94]
			16.58 (0.6 Ω 3.25 V)	7.2%		
	18650 1.50 Ah 5S3P <sup>b</sup>	−15.0~10.0	2.50	-	Temperature gradient 14.49 °C	[101]

Table 12. Cont.

Heating Techniques	Battery Type	Temperature Range (°C)	Rate of Temperature Rise (°C/min)	Capacity Used	Other Key Parameters	Ref.
PCM preheating	18650 1.50 Ah 5S3P <sup>b</sup>	−15.0~10.0	0.74	-	Temperature gradient 2.82 °C	[101]
Liquid preheating	Prismatic 12 cells	−28~25	4.18	-	Temperature gradient <4.00 °C	[100]
Electric heating element heating	Pack 50.00 Ah 5P	−20.0~20.0	5.85 (heating film) 4.78 (UMHP)	-	-	[102]
Hybrid heating	NCM Laminated 8.00 Ah	−30.0~2.0	31.13	-	Temperature gradient 13.38 °C Capacity fade 0.79% (500 cycle)	[103]
	NCMA <sup>c</sup> 18650 3.20 Ah 5S2P	−10.0~20.0	17.14	4.4%	Temperature gradient 3.58 °C	[104]
	Laminated 13.50 Ah	−20.0~0.0	11.22	4.0%	-	[105]
	NCM Laminated 8.00 Ah	−29.8~−2.0	32.49	10.9%	Capacity fade 1.02% (500 cycle) 3.58% (2000 cycle) Temperature gradient 14.79 °C	[106]

<sup>a</sup> All-climate battery (ACB); <sup>b</sup> 5S3P batteries (5 cells in series and 3 cells in parallel); <sup>c</sup> LiNiMnCoAlO<sub>2</sub> (NCMA).

## 5. Conclusions and Perspectives

We systematically reviewed the state-of-the-art research about performance decrease, modeling, and heating of LIBs at low temperatures, and attempted to provide the quantitative results to motivate effective solutions for addressing the challenge of low-temperature applications of LIBs. The conclusions and perspectives are shown in Figure 20.

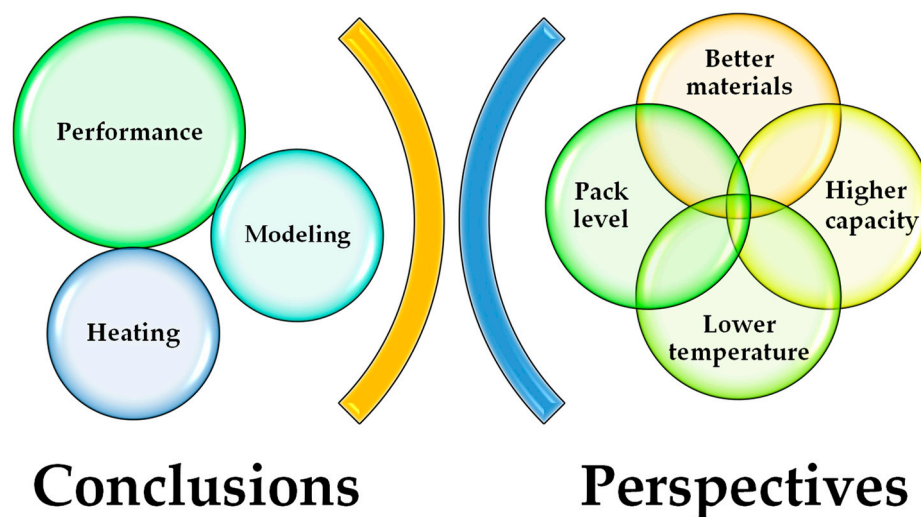


Figure 20. Conclusions and perspectives.

Firstly, the performance of LIBs at low temperatures is summarized, including four perspectives: charging, discharging, EIS, and degradation. Charging at low temperatures results in lower charging capacity and higher midpoint voltage, reaching the endpoint voltage more quickly than at room temperature. For example, the charge capacity of the LIB in [60] drops to 50.92% at −20 °C, and the midpoint voltage (charge capacity) rises by 0.313 V. In terms of discharge, the capacity of the battery decreases exponentially with the decreasing temperature. The EIS shows that the ohmic internal resistance and charge transfer impedance of the battery increase as the temperature decreases, and the

diffusion process slows down. In terms of degradation, the degradation of the battery at low temperature is more serious than at room temperature, and the maximum degradation rate can be 47 times that of room temperature, which increases exponentially as the temperature decreases.

Secondly, in terms of low-temperature battery models, this paper summarizes ECM, electrochemical models, and aging models. The conventional ECMs are often improved by investigating the dependence of the correlation parameter (SOC, R, C, etc.) on temperature, resulting in coupled thermal first- and second-order ECMs. Meanwhile, more accurate low-temperature battery models can be obtained by embedding the Butler–Volmer equation, Nernst equation, and Arrhenius equation into the ECM [79,80]. In terms of electrochemical modeling, some studies have added a lumped thermal model to the P2D model and modified relevant equations or parameters to make it suitable for low-temperature scenarios. Electrochemical modeling involves many parameters, and when building low-temperature electrochemical models, it is often necessary to consider temperature-sensitive parameters so that they change adaptively with temperature to improve the accuracy of the model. In terms of aging modeling, researchers identified the loss of active materials, lithium ions, and the reduction of accessible surface area as the main causes of battery degradation at low temperatures, and that the loss of conductivity at low temperatures is three times higher than at room temperature. The low-temperature battery aging model can be divided into two stages based on the rate of capacity decline. Stage 1 (0–10%, slower): temperature has the greatest effect on battery aging, and Stage 2 (10–20%, faster): the charging cut-off voltage increases the capacity decay [91]. Depending on the type of battery, decline can be divided into calendar aging and cyclic aging; the former shows a low degradation with a low degradation model factor at low temperatures, the latter shows a high degradation and the corresponding modeled coefficients accounted for more [92]. The idea of categorical discussion is well represented in the aging modeling at low temperatures.

Finally, this paper summarizes the heating methods that can enhance the low-temperature performance of LIBs. The low-temperature heating of LIBs can be generally divided into internal heating, external heating, and hybrid heating. Classified from the perspective of physical structure, internal heating includes current-excited heating and SHLB technology. We concluded that the higher the current amplitude, the higher the heat production of the battery and the faster the temperature rise of the battery, but a too-high current may cause the voltage of the battery to exceed the safety voltage, resulting in overcharging or overdischarging of the battery, which may lead to accelerated degradation or even safety hazards. Therefore, a high heating current is usually expected for increased heating rates, but the degradation boundary needs to be taken into account. SHLB technology has the advantage of fast and efficient heating with the nickel foil pre-embedded inside the battery, and it only takes 20 s to go from  $-20\text{ }^{\circ}\text{C}$  to  $0\text{ }^{\circ}\text{C}$  with 3.8% of the battery capacity consumption, but the change of the battery structure leads to the reduced energy density of the battery, and at the same time, higher requirements for the battery production process, which also results in the potential safety risks. External heating methods mainly include air heating, liquid heating, PCM heating, and electric heating element heating. Generally, the heating efficiency is low, the heating rate is slow, and the uniformity is poor. External heating is relatively safe due to the slow heating, and care needs to be taken to keep the heating liquid airtight. Hybrid heating is a combination of the internal heating and external heating methods, which can improve the heating rate and efficiency of the LIB, reduce the temperature gradient of the LIB, and at the same time, have less impact on the LIB life, which can better ensure the reliability and stability of the system. For example, the hybrid heating method proposed in [106] has a temperature rise rate of up to  $32.49\text{ }^{\circ}\text{C}/\text{min}$ , and the capacity fade of 2000 cycles is only 3.58%. Therefore, the hybrid heating method is a more promising low-temperature heating method for LIBs.

With the quantification results, the prospects can be summarized as directions for future research:

1. More promising materials. Better battery materials with good low-temperature performance are expected to develop to meet the current demand for batteries with excellent low-temperature performance and to fundamentally improve the low-temperature performance of Li-ion batteries. (1) It is shown that high activation energies  $E_a$  and the difference in activation energy  $E_a$  between the cathode and the anode are the reasons for low-temperature-induced capacity fade at low currents. Electrode materials can be prepared and screened from the perspective of activation energy. (2) After electrochemical modeling analysis, it was shown that the influence of negative electrode parameters on the battery performance at low temperature is much larger than that of positive electrode parameters, while the influence of electrode porosity and initial liquid lithium-ion concentration on the battery performance is negligible. More attention should be given to low-temperature negative electrode materials exploration. (3) At present, the mechanical properties such as stiffness of battery materials at low temperature are less explored, which can be given proper attention.

2. More comprehensive modeling. The current low-temperature models have a narrow temperature range, making it difficult to adapt to a wide range of application scenarios. At the same time, the factors considered are mostly focused on the influence of SOC and current. More factors in a wider temperature range should be explored to improve the performance of the battery and promote better development of EVs. (1) With the expansion of applications in special fields such as deep-sea exploration, special working conditions have placed higher demands on the low-temperature performance of LIBs. Experiments and modeling of LIBs at lower temperatures ( $-20\sim-40\text{ }^\circ\text{C}$ ) should be carried out. (2) As the battery is used, the parameters of the battery will change with aging and should not be only limited to the effects of current, SOC, and T. Therefore, the complex coupling characteristics of the model should be considered. (3) In addition, exploration of battery pack inconsistency at low temperatures should also be carried out. (4) Finally, the electrochemical modeling of batteries at low temperatures is less studied, and there is a lack of boundary conditions for the charging and discharging of LIBs in a wide range of temperatures, so in-depth research on the mechanism of low-temperature batteries should be carried out.

3. More balanced heating method. At present, considering the cost, energy density, safety performance, and many other circumstances, it is still necessary to conduct experiments and research in the battery anode and electrolyte, etc. Therefore, it is necessary to develop heating methods with better overall indexes to meet the use of EVs at low temperatures. (1) With the development of EVs and industry demand, the single-battery capacity is now larger, and the problem of adaptability of larger-capacity batteries in low-temperature environments needs to be solved urgently. (2) Future research should focus more on the battery pack level, which can have problems such as high current and temperature inconsistency. In order to accelerate the heating method from laboratory to industrialization, more efforts should be made on the inhomogeneity of the battery pack and implementation of heating methods. (3) The low-temperature heating method for LIBs that optimizes the heating rate, heating energy consumption, temperature uniformity, and life degradation is the focus of future research.

**Author Contributions:** Conceptualization, B.S.; investigation, D.S.; project administration, H.R.; writing—original draft, X.Q.; writing—review and editing, H.R. All authors have read and agreed to the published version of the manuscript.

**Funding:** This research was funded by the National Natural Science Foundation of China (52177206) and the Joint Fund of Ministry of Education of China for Equipment Pre-research (Grant No. 8091B022130).

**Data Availability Statement:** Not applicable.

**Conflicts of Interest:** The authors declare no conflict of interest.

## Nomenclature

$D_1$	Diffusion coefficient of $\text{Li}^+$ in the electrolyte
$D_2$	Diffusion coefficient
$D_{a,n}$	Bulk diffusion coefficient of $\text{Li}^+$ in anode
$D_{s,i}$	Solid-phase diffusivity ( $i = n, p$ )
$k_{0,i}$	Reaction rate constant
$k_{an}$	Reaction rate constant of anode
$k_{cat}$	Reaction rate constant of cathode
$k_n$	Lumped charge transfer constant
$P_{act,n}$	Negative electrode reaction kinetics control parameters
$P_{act,p}$	Positive electrode reaction kinetics control parameters
$P_{comp}$	Positive proportional coefficient of liquid-phase diffusion
$p_{e,n}^{dyn}$	Dynamic control constant of negative electrode solution-phase diffusion
$p_{e,n}^{ste}$	Steady-state control constant of negative electrode solution-phase diffusion
$p_{e,p}^{dyn}$	Dynamic control constant of positive electrode solution-phase diffusion
$p_{e,p}^{ste}$	Steady-state control constant of positive electrode solution-phase diffusion
$p_{s,n}^{dyn}$	Dynamic control constant of negative electrode solid-phase diffusion
$p_{s,p}^{dyn}$	Dynamic control constant of positive electrode solid-phase diffusion
$R_{ohm}$	Ohmic resistance
$v$	Thermodynamic factor
$\kappa_1$	Ionic conductivity of the electrolyte
$v_1$	Thermodynamic factor of the electrolyte
$\sigma_2$	Ionic conductivity
$\tau_e$	Liquid-phase diffusion time constant
$\tau_n$	Solid-phase diffusion time constant of electrodes

## Abbreviations

AC	Alternating current
ACB	All-climate battery
AE	Average error
APE	Average percentage error
BEVs	Battery electric vehicles
CCD	Constant-current discharge
CEI	Cathode electrolyte interphase
CFD	Computational fluid dynamics
CNN-LSTM	Convolutional neural network and long short-term memory
cPCM	Composite phase-change materials
CPV	Constant polarization voltage
CSC	Constant sinusoidal current
CVD	Constant-voltage discharge
DC	Direct current
DOD	Depth of discharge
DV	Differential voltage
ECM	Equivalent circuit model
EIS	Electrochemical impedance spectroscopy
EVs	Electric vehicles
FUDS	Federal urban driving schedule
HPPC	Hybrid pulse power characteristic
IC	Incremental capacity
LCO	$\text{LiCoO}_2$
LFP	$\text{LiFePO}_4$
LIBs	Lithium-ion batteries
LMO	$\text{LiMn}_2\text{O}_4$
LNO	$\text{LiNiO}_2$
LT	Low temperature
LTO	$\text{Li}_4\text{Ti}_5\text{O}_{12}$
LVP	$\text{Li}_3\text{V}_2(\text{PO}_4)_3$

MAE	Mean absolute errors
MAEE	Maximum absolute estimation error
ME	Maximum error
MPE	Maximum percentage error
MRE	Maximum relative error
NA	Not available
NCA	$\text{LiNi}_{1-x-y}\text{Co}_x\text{Al}_y\text{O}_2$
NCM	$\text{LiNi}_{1-x-y}\text{Co}_x\text{Mn}_y\text{O}_2$
NCMA	$\text{LiNiMnCoAlO}_2$
NCO	$\text{LiNi}_{0.8}\text{Co}_{0.2}\text{O}_2$
OCV	Open-circuit voltage
P2D	Pseudo-two-dimensional
PCM	Phase-change material
PHEVs	Plug-in hybrid electric vehicles
RC	Resistance and capacitance
RMSE	Root mean square error
RT	Room temperature
SD	Standard deviation
SEI	Solid electrolyte interphase
SHLB	Self-heating lithium-ion battery
SOC	State of charge
SP	Single particle
UMHP	Ultra-thin micro-heat pipe

## References

1. New Energy Vehicle Industry Plan (2021–2035). Available online: [https://www.ndrc.gov.cn/fggz/fzzlgh/gjjzqgh/202111/t20211101\\_1302487.html](https://www.ndrc.gov.cn/fggz/fzzlgh/gjjzqgh/202111/t20211101_1302487.html) (accessed on 15 August 2023).
2. Deal Confirms Zero-Emissions Target for New Cars and Vans in 2035. Available online: <https://www.europarl.europa.eu/news/en/press-room/20221024IPR45734/deal-confirms-zero-emissions-target-for-new-cars-and-vans-in-2035> (accessed on 15 August 2023).
3. FACT SHEET: President Biden Announces Steps to Drive American Leadership Forward on Clean Cars and Trucks. Available online: <https://www.whitehouse.gov/briefing-room/statements-releases/2021/08/05/fact-sheet-president-biden-announces-steps-to-drive-american-leadership-forward-on-clean-cars-and-trucks/> (accessed on 15 August 2023).
4. Global EV Data Explorer. Available online: <https://www.iea.org/data-and-statistics/data-tools/global-ev-data-explorer> (accessed on 15 August 2023).
5. Zhang, S.S.; Xu, K.; Jow, T.R. Charge and discharge characteristics of a commercial LiCoO<sub>2</sub>-based 18650 Li-ion battery. *J. Power Sources* **2006**, *160*, 1403–1409. [[CrossRef](#)]
6. IEA. *Global EV Outlook 2019: Scaling-Up the Transition to Electric Mobility*; OECD: Paris, France, 2019.
7. Ouyang, M.; Chu, Z.; Lu, L.; Li, J.; Han, X.; Feng, X.; Liu, G. Low temperature aging mechanism identification and lithium deposition in a large format lithium iron phosphate battery for different charge profiles. *J. Power Sources* **2015**, *286*, 309–320. [[CrossRef](#)]
8. Zhang, G.; Wei, X.; Tang, X.; Zhu, J.; Chen, S.; Dai, H. Internal short circuit mechanisms, experimental approaches and detection methods of lithium-ion batteries for electric vehicles: A review. *Renew. Sustain. Energy Rev.* **2021**, *141*, 110790. [[CrossRef](#)]
9. Electric Vehicle Sales Leapt 55% in 2022—Here’s Where That Growth Was Strongest. Available online: <https://www.weforum.org/agenda/2023/05/electric-vehicles-ev-sales-growth-2022/> (accessed on 15 August 2023).
10. China Meteorological Administration. *China Meteorological Yearbook 2021*; China Meteorological Press: Beijing, China, 2021.
11. Buidin, T.I.C.; Mariasiu, F. Battery Thermal Management Systems: Current Status and Design Approach of Cooling Technologies. *Energies* **2021**, *14*, 4879. [[CrossRef](#)]
12. Xu, W.; Chan, K.W.; Or, S.W.; Ho, S.L.; Liu, M. A Low-Harmonic Control Method of Bidirectional Three-Phase Z-Source Converters for Vehicle-to-Grid Applications. *IEEE Trans. Transp. Electr.* **2020**, *6*, 464–477. [[CrossRef](#)]
13. Liu, J.; Xu, W.; Chan, K.W.; Liu, M.; Zhang, X.; Chan, N.H.L. A Three-Phase Single-Stage AC–DC Wireless-Power-Transfer Converter with Power Factor Correction and Bus Voltage Control. *IEEE J. Emerg. Sel. Top. Power Electron.* **2019**, *8*, 1782–1800. [[CrossRef](#)]
14. Zhu, G.; Wen, K.; Lv, W.; Zhou, X.; Liang, Y.; Yang, F.; Chen, Z.; Zou, M.; Li, J.; Zhang, Y.; et al. Materials insights into low-temperature performances of lithium-ion batteries. *J. Power Sources* **2015**, *300*, 29–40. [[CrossRef](#)]
15. Vlahinos, A.; Pesaran, A.A. Energy Efficient Battery Heating in Cold Climates. *SAE Trans.* **2002**, *111*, 826–833.
16. Osmani, K.; Alkhedher, M.; Ramadan, M.; Choi, D.S.; Li, L.K.; Doranehgard, M.H.; Olabi, A.G. Recent progress in the thermal management of lithium-ion batteries. *J. Clean Prod.* **2023**, *389*, 136024. [[CrossRef](#)]

17. Chen, Z.; Danilov, D.L.; Eichel, R.A.; Notten, P.H. Porous Electrode Modeling and its Applications to Li-Ion Batteries. *Adv. Energy Mater.* **2022**, *12*, 2201506. [[CrossRef](#)]
18. Planella, F.B.; Ai, W.; Boyce, A.M.; Ghosh, A.; Korotkin, I.; Sahu, S.; Sulzer, V.; Timms, R.; Tranter, T.G.; Zyskin, M.; et al. A continuum of physics-based lithium-ion battery models reviewed. *Prog. Energy* **2022**, *4*, 042003. [[CrossRef](#)]
19. Xu, L.; Deng, Z.; Xie, Y.; Hu, X. Review on Research Progress in High-fidelity Modeling, Parameter Identification and Lifetime Prognostics of Lithium-ion Battery. *Chin. J. Mech. Eng.* **2022**, *58*, 19–36.
20. Liu, K.; Gao, Y.; Zhu, C.; Li, K.; Fei, M.; Peng, C.; Zhang, X.; Han, Q.L. Electrochemical modeling and parameterization towards control-oriented management of lithium-ion batteries. *Control Eng. Pract.* **2022**, *124*, 105176. [[CrossRef](#)]
21. Cui, Z.; Dai, J.; Sun, J.; Li, D.; Wang, L.; Wang, K. Hybrid methods using neural network and Kalman filter for the state of charge estimation of lithium-ion battery. *Math. Probl. Eng.* **2022**, *2022*, 9616124. [[CrossRef](#)]
22. Tian, J.; Xiong, R.; Shen, W.; Sun, F. Fractional order battery modelling methodologies for electric vehicle applications: Recent advances and perspectives. *Sci. China Technol. Sci.* **2020**, *63*, 2211–2230. [[CrossRef](#)]
23. Hu, X.; Zheng, Y.; Howey, D.A.; Perez, H.; Foley, A.; Pecht, M. Battery warm-up methodologies at subzero temperatures for automotive applications: Recent advances and perspectives. *Prog. Energy Combust. Sci.* **2020**, *77*, 100806. [[CrossRef](#)]
24. Wang, Y.; Zhang, X.; Chen, Z. Low temperature preheating techniques for Lithium-ion batteries: Recent advances and future challenges. *Appl. Energy* **2022**, *313*, 118832. [[CrossRef](#)]
25. Lin, C.; Kong, W.; Tian, Y.; Wang, W.; Zhao, M. Heating Lithium-Ion Batteries at Low Temperatures for Onboard Applications: Recent Progress, Challenges and Prospects. *Automot. Innov.* **2022**, *5*, 3–17. [[CrossRef](#)]
26. Zhu, C.; Du, L.; Guo, B.; Fan, G.; Lu, F.; Zhang, H.; Liu, K.; Zhang, X. Internal Heating Techniques for Lithium-ion Batteries at Cold Climates: An Overview for Automotive Applications. *IEEE Trans. Transp. Electrification* **2022**. [[CrossRef](#)]
27. Ruan, H.; Barreras, J.V.; Steinhardt, M.; Jossen, A.; Offer, G.J.; Wu, B. The heating triangle: A quantitative review of self-heating methods for lithium-ion batteries at low temperatures. *J. Power Sources* **2023**, *581*, 233484. [[CrossRef](#)]
28. Belgibayeva, A.; Rakhmetova, A.; Rakhmatkyzy, M.; Kairova, M.; Mukushev, I.; Issatayev, N.; Kalimuldina, G.; Nurpeissova, A.; Sun, Y.K.; Bakenov, Z. Lithium-ion batteries for low-temperature applications: Limiting factors and solutions. *J. Power Sources* **2023**, *557*, 232550. [[CrossRef](#)]
29. Luo, H.; Wang, Y.; Feng, Y.-H.; Fan, X.-Y.; Han, X.; Wang, P.-F. Lithium-Ion Batteries under Low-Temperature Environment: Challenges and Prospects. *Materials* **2022**, *15*, 8166. [[CrossRef](#)] [[PubMed](#)]
30. Chen, X.; Gong, Y.; Li, X.; Zhan, F.; Liu, X.; Ma, J. Perspective on low-temperature electrolytes for LiFePO<sub>4</sub>-based lithium-ion batteries. *Int. J. Miner. Metall. Mater.* **2023**, *30*, 1–13. [[CrossRef](#)]
31. Mei, P.; Zhang, Y.; Zhang, W. Low-temperature lithium-ion batteries: Challenges and progress of surface/interface modifications for advanced performance. *Nanoscale* **2023**, *15*, 987–997. [[CrossRef](#)]
32. Su, X.; Xu, Y.; Wu, Y.; Li, H.; Yang, J.; Liao, Y.; Qu, R.; Zhang, Z. Liquid electrolytes for low-temperature lithium batteries: Main limitations, current advances, and future perspectives. *Energy Storage Mater.* **2023**, *56*, 642–663. [[CrossRef](#)]
33. Hubble, D.; Brown, D.E.; Zhao, Y.; Fang, C.; Lau, J.; McCloskey, B.D.; Liu, G. Liquid electrolyte development for low-temperature lithium-ion batteries. *Energy Environ. Sci.* **2022**, *15*, 550–578. [[CrossRef](#)]
34. Lin, W.; Zhu, M.; Fan, Y.; Wang, H.; Tao, G.; Ding, M.; Liu, N.; Yang, H.; Wu, J.; Fang, J.; et al. Low temperature lithium-ion batteries electrolytes: Rational design, advancements, and future perspectives. *J. Alloys Compd.* **2022**, *905*, 164163. [[CrossRef](#)]
35. Zheng, Y.; Qian, T.; Zhou, J.; Liu, J.; Wang, Z.; Wang, S.; Wang, Y.; Yan, C. Advanced Strategies for Improving Lithium Storage Performance under Cryogenic Conditions. *Adv. Energy Mater.* **2023**, *13*, 2203719. [[CrossRef](#)]
36. Sun, J.; Ye, L.; Zhao, X.; Zhang, P.; Yang, J. Electronic Modulation and Structural Engineering of Carbon-Based Anodes for Low-Temperature Lithium-Ion Batteries: A Review. *Molecules* **2023**, *28*, 2108. [[CrossRef](#)]
37. Li, J.; Zuo, P. Research progress on low-temperature graphite anode and electrolyte optimization for lithium-ion batteries. *Sci. Sin. Chim.* **2022**, *52*, 1824–1833. [[CrossRef](#)]
38. Worku, B.E.; Zheng, S.; Wang, B. Review of low-temperature lithium-ion battery progress: New battery system design imperative. *Int. J. Energy Res.* **2022**, *46*, 14609–14626. [[CrossRef](#)]
39. Pang, X.; An, B.; Zheng, S.; Wang, B. Cathode materials of metal-ion batteries for low-temperature applications. *J. Alloys Compd.* **2022**, *912*, 165142. [[CrossRef](#)]
40. Mennel, J.A.; Chidambaram, D. A review on the development of electrolytes for lithium-based batteries for low temperature applications. *Front. Energy* **2022**, *17*, 43–71. [[CrossRef](#)]
41. Han, F.; Chang, Z.; Zhao, J.; Wang, R.; Ding, H.; Lu, S. Research progress in low-temperature discharge performance of Ni-rich ternary lithium-ion batteries. *Cailiao Gongcheng* **2022**, *50*, 1–17.
42. Zhang, D.; Tan, C.; Ou, T.; Zhang, S.; Li, L.; Ji, X. Constructing advanced electrode materials for low-temperature lithium-ion batteries: A review. *Energy Rep.* **2022**, *8*, 4525–4534. [[CrossRef](#)]
43. Selinis, P.; Farmakis, F. A review on the anode and cathode materials for lithium-ion batteries with improved subzero temperature performance. *J. Electrochem. Soc.* **2022**, *169*, 010526. [[CrossRef](#)]
44. Na, Y.; Sun, X.; Fan, A.; Cai, S.; Zheng, C. Methods for enhancing the capacity of electrode materials in low-temperature lithium-ion batteries. *Chin. Chem. Lett.* **2021**, *32*, 973–982. [[CrossRef](#)]
45. Guo, R.; Han, W. The effects of electrolytes, electrolyte/electrode interphase and binders on lithium-ion batteries at low temperature. *Mater. Today Sustain.* **2022**, *19*, 100187. [[CrossRef](#)]

46. Meng, F.; Xiong, X.; Tan, L.; Yuan, B.; Hu, R. Strategies for improving electrochemical reaction kinetics of cathode materials for subzero-temperature Li-ion batteries: A review. *Energy Storage Mater.* **2022**, *44*, 390–407. [[CrossRef](#)]
47. Zhang, N.; Deng, T.; Zhang, S.; Wang, C.; Chen, L.; Wang, C.; Fan, X. Critical Review on Low-Temperature Li-Ion/Metal Batteries. *Adv. Mater.* **2022**, *34*, 2107899. [[CrossRef](#)]
48. Kulova, T.L.; Skundin, A.M. A critical review of electrode materials and electrolytes for low-temperature lithium-ion batteries. *Int. J. Electrochem. Sci.* **2020**, *15*, 8638–8661. [[CrossRef](#)]
49. Collins, G.A.; Geaney, H.; Ryan, K.M. Alternative anodes for low temperature lithium-ion batteries. *J. Mater. Chem. A* **2021**, *9*, 14172–14213. [[CrossRef](#)]
50. Hou, J.; Yang, M.; Wang, D.; Zhang, J. Fundamentals and challenges of lithium ion batteries at temperatures between  $-40$  and  $60$  °C. *Adv. Energy Mater.* **2020**, *10*, 1904152. [[CrossRef](#)]
51. Zhang, S.S.; Xu, K.; Jow, T.R. Electrochemical impedance study on the low temperature of Li-ion batteries. *Electrochim. Acta* **2004**, *49*, 1057–1061. [[CrossRef](#)]
52. Zhang, S.S.; Xu, K.; Jow, T.R. The low temperature performance of Li-ion batteries. *J. Power Sources* **2003**, *115*, 137–140. [[CrossRef](#)]
53. Zhang, S.S.; Xu, K.; Jow, T.R. Low temperature performance of graphite electrode in Li-ion cells. *Electrochim. Acta* **2003**, *48*, 241–246. [[CrossRef](#)]
54. Ren, D.; Smith, K.; Guo, D.; Han, X.; Feng, X.; Lu, L.; Ouyang, M.; Li, J. Investigation of Lithium Plating-Stripping Process in Li-ion Batteries at low temperature Using an Electrochemical Model. *J. Electrochem. Soc.* **2018**, *165*, A2167. [[CrossRef](#)]
55. Singer, J.P.; Birke, K.P. Kinetic study of low temperature capacity fading in Li-ion cells. *J. Energy Storage* **2017**, *13*, 129–136. [[CrossRef](#)]
56. Rauhala, T.; Jalkanen, K.; Romann, T.; Lust, E.; Omar, N.; Kallio, T. Low-temperature aging mechanisms of commercial graphite/LiFePO<sub>4</sub> cells cycled with a simulated electric vehicle load profile—A post-mortem study. *J. Energy Storage* **2018**, *20*, 344–356. [[CrossRef](#)]
57. Kucinskis, G.; Bozorgchenani, M.; Feinauer, M.; Kasper, M.; Wohlfahrt-Mehrens, M.; Waldmann, T. Arrhenius plots for Li-ion battery ageing as a function of temperature, C-rate, and ageing state—An experimental study. *J. Power Sources* **2022**, *549*, 232129. [[CrossRef](#)]
58. Qiao, Y.Q.; Tu, J.P.; Wang, X.L.; Gu, C.D. The low and high temperature electrochemical performances of Li<sub>3</sub>V<sub>2</sub>(PO<sub>4</sub>)<sub>3</sub>/C cathode material for Li-ion batteries. *J. Power Sources* **2012**, *199*, 287–292. [[CrossRef](#)]
59. Qiu, B.; Wang, J.; Xia, Y.; Wei, Z.; Han, S.; Liu, Z. Temperature dependence of the initial coulombic efficiency in Li-rich layered Li[Li<sub>0.144</sub>Ni<sub>0.136</sub>Co<sub>0.136</sub>Mn<sub>0.544</sub>]O<sub>2</sub> oxide for lithium-ions batteries. *J. Power Sources* **2014**, *268*, 517–521. [[CrossRef](#)]
60. Hamenu, L.; Lee, H.S.; Latifatu, M.; Kim, K.M.; Park, J.; Baek, Y.G.; Ko, J.M.; Kaner, R.B. Lithium-silica nanosalt as a low-temperature electrolyte additive for lithium-ion batteries. *Curr. Appl. Phys.* **2016**, *16*, 611–617. [[CrossRef](#)]
61. Chen, K.; Li, X. Accurate determination of battery discharge characteristics—A comparison between two battery temperature control methods. *J. Power Sources* **2014**, *247*, 961–966. [[CrossRef](#)]
62. Wu, G.; Li, C.; Jiao, D.; Liu, Y.; Hao, C.; Zhang, Y.; Yu, H.; Zhang, M. State of Charge Estimation for Li-Ion Battery Based on an Improved Peukert's Equation with Temperature Correction Factor. In Proceedings of the 2016 IEEE Vehicle Power and Propulsion Conference (VPPC), Hangzhou, China, 17–20 October 2016; pp. 1–4.
63. Jaguemont, J.; Boulon, L.; Dubé, Y. Characterization and Modeling of a Hybrid-Electric-Vehicle Lithium-Ion Battery Pack at Low Temperatures. *IEEE Trans. Veh. Technol.* **2015**, *65*, 1–14. [[CrossRef](#)]
64. Ge, H.; Aoki, T.; Ikeda, N.; Suga, S.; Isobe, T.; Li, Z.; Tabuchi, Y.; Zhang, J. Investigating Lithium Plating in Lithium-Ion Batteries at Low Temperatures Using Electrochemical Model with NMR Assisted Parameterization. *J. Electrochem. Soc.* **2017**, *164*, A1050. [[CrossRef](#)]
65. Momma, T.; Matsunaga, M.; Mukoyama, D.; Osaka, T. Ac impedance analysis of lithium ion battery under temperature control. *J. Power Sources* **2012**, *216*, 304–307. [[CrossRef](#)]
66. Wu, W.; Ma, R.; Liu, J.; Liu, M.; Wang, W.; Wang, Q. Impact of low temperature and charge profile on the aging of lithium-ion battery: Non-invasive and post-mortem analysis. *Int. J. Heat Mass Transf.* **2021**, *170*, 121024. [[CrossRef](#)]
67. Tippmann, S.; Walper, D.; Balboa, L.; Spier, B.; Bessler, W.G. Low-temperature charging of lithium-ion cells part I: Electrochemical modeling and experimental investigation of degradation behavior. *J. Power Sources* **2014**, *252*, 305–316. [[CrossRef](#)]
68. Guo, S.; Xiong, R.; Shen, W.; Sun, F. Aging investigation of an echelon internal heating method on a three-electrode lithium ion cell at low temperatures. *J. Energy Storage* **2019**, *25*, 100878. [[CrossRef](#)]
69. Laforgue, A.; Yuan, X.Z.; Platt, A.; Brueckner, S.; Perrin-Sarazin, F.; Toupin, M.; Huot, J.Y.; Mokrini, A. Comparative investigation of the impact of fast charging at low temperature on commercial Li-ion cells. *J. Power Sources* **2022**, *524*, 231071. [[CrossRef](#)]
70. Omar, N.; Monem, M.A.; Firouz, Y.; Salminen, J.; Smekens, J.; Hegazy, O.; Gaulous, H.; Mulder, G.; Van den Bossche, P.; Coosemans, T.; et al. Lithium iron phosphate based battery—Assessment of the aging parameters and development of cycle life model. *Appl. Energy* **2014**, *113*, 1575–1585. [[CrossRef](#)]
71. Zhang, G.; Wei, X.; Han, G.; Dai, H.; Zhu, J.; Wang, X.; Tang, X.; Ye, J. Lithium plating on the anode for lithium-ion batteries during long-term low temperature cycling. *J. Power Sources* **2021**, *484*, 229312. [[CrossRef](#)]
72. Petzl, M.; Kasper, M.; Danzer, M.A. Lithium plating in a commercial lithium-ion battery—A low-temperature aging study. *J. Power Sources* **2015**, *275*, 799–807. [[CrossRef](#)]

73. Waldmann, T.; Wilka, M.; Kasper, M.; Fleischhammer, M.; Wohlfahrt-Mehrens, M. Temperature dependent ageing mechanisms in Lithium-ion batteries—A Post-Mortem study. *J. Power Sources* **2014**, *262*, 129–135. [[CrossRef](#)]
74. Storch, M.; Fath, J.P.; Sieg, J.; Vrankovic, D.; Krupp, C.; Spier, B.; Riedel, R. Temperature and Lithium Concentration Gradient Caused Inhomogeneous Plating in Large-format Lithium-ion Cells. *J. Energy Storage* **2021**, *41*, 102887. [[CrossRef](#)]
75. Waldmann, T.; Hogg, B.I.; Kasper, M.; Grolleau, S.; Couceiro, C.G.; Trad, K.; Matadi, B.P.; Wohlfahrt-Mehrens, M. Interplay of Operational Parameters on Lithium Deposition in Lithium-Ion Cells: Systematic Measurements with Reconstructed 3-Electrode Pouch Full Cells. *J. Electrochem. Soc.* **2016**, *163*, A1232. [[CrossRef](#)]
76. Waldmann, T.; Quinn, J.B.; Richter, K.; Kasper, M.; Tost, A.; Klein, A.; Wohlfahrt-Mehrens, M. Electrochemical, Post-Mortem, and ARC Analysis of Li-Ion Cell Safety in Second-Life Applications. *J. Electrochem. Soc.* **2017**, *164*, A3154. [[CrossRef](#)]
77. Kamrueng, C.; Kittiratsatcha, S.; Polmai, S. A Number of RC Pairs Consideration of Electrical Equivalent Circuit Model of Li-ion Battery. In Proceedings of the 2020 6th International Conference on Engineering, Applied Sciences and Technology (ICEAST), Chiang Mai, Thailand, 1–4 July 2020; pp. 1–4.
78. Das, D.; Sharma, S.; Jana, M.; Basu, S. A modified equivalent circuit model to capture low temperature effects in Li ion batteries. In Proceedings of the 2019 IEEE Transportation Electrification Conference (ITEC-India), Bengaluru, India, 17–19 December 2019; pp. 1–6.
79. Zhu, J.; Knapp, M.; Darma, M.S.D.; Fang, Q.; Wang, X.; Dai, H.; Wei, X.; Ehrenberg, H. An improved electro-thermal battery model complemented by current dependent parameters for vehicular low temperature application. *Appl. Energy* **2019**, *248*, 149–161. [[CrossRef](#)]
80. Chen, A.; Zhang, W.; Zhang, C.; Huang, W.; Liu, S. A Temperature and Current Rate Adaptive Model for High-Power Lithium-Titanate Batteries Used in Electric Vehicles. *IEEE Trans. Ind. Electron.* **2019**, *67*, 9492–9502. [[CrossRef](#)]
81. Jiang, J.; Ruan, H.; Sun, B.; Zhang, W.; Gao, W.; Wang, L.Y.; Zhang, L. A reduced low-temperature electro-thermal coupled model for lithium-ion batteries. *Appl. Energy* **2016**, *177*, 804–816. [[CrossRef](#)]
82. Fang, Y.; Zhang, Q.; Zhang, H.; Xu, W.; Wang, L.; Shen, X.; Yun, F.; Cui, Y.; Wang, L.; Zhang, X. State-of-charge estimation technique for lithium-ion batteries by means of second-order extended Kalman filter and equivalent circuit model: Great temperature robustness state-of-charge estimation. *IET Power Electron.* **2021**, *14*, 1515–1528. [[CrossRef](#)]
83. Doyle, M.; Fuller, T.F.; Newman, J. Modeling of Galvanostatic Charge and Discharge of the Lithium/Polymer/Insertion Cell. *J. Electrochem. Soc.* **1993**, *140*, 1526. [[CrossRef](#)]
84. Gholami, J.; Barzoki, M.F. Electrochemical modeling and parameter sensitivity of lithium-ion battery at low temperature. *J. Energy Storage* **2021**, *43*, 103189. [[CrossRef](#)]
85. Wang, D.; Huang, H.; Tang, Z.; Zhang, Q.; Yang, B.; Zhang, B. A lithium-ion battery electrochemical–thermal model for a wide temperature range applications. *Electrochim. Acta* **2020**, *362*, 137118. [[CrossRef](#)]
86. An, Z.; Jia, L.; Wei, L.; Dang, C.; Peng, Q. Investigation on lithium-ion battery electrochemical and thermal characteristic based on electrochemical-thermal coupled model. *Appl. Therm. Eng.* **2018**, *137*, 792–807. [[CrossRef](#)]
87. Xu, S.; Wang, Y.; Shao, J.; Li, J.; Yu, Q. An electrochemical-thermal coupling model for prismatic lithium-ion batteries over wide temperature range. *Appl. Therm. Eng.* **2022**, *217*, 119282. [[CrossRef](#)]
88. Remmlinger, J.; Tippmann, S.; Buchholz, M.; Dietmayer, K. Low-temperature charging of lithium-ion cells Part II: Model reduction and application. *J. Power Sources* **2014**, *254*, 268–276. [[CrossRef](#)]
89. Li, C.; Cui, N.; Wang, C.; Zhang, C. Simplified electrochemical lithium-ion battery model with variable solid-phase diffusion and parameter identification over wide temperature range. *J. Power Sources* **2021**, *497*, 229900. [[CrossRef](#)]
90. Liu, H.; Wang, Y.; Li, W.; Shao, F.; He, M. Decay mechanism and capacity prediction of lithium-ion batteries under low-temperature near-adiabatic condition. *Inorg. Chem. Commun.* **2022**, *137*, 109151. [[CrossRef](#)]
91. You, H.; Dai, H.; Li, L.; Wei, X.; Han, G. Charging Strategy Optimization at Low Temperatures for Li-Ion Batteries Based on Multi-Factor Coupling Aging Model. *IEEE Trans. Veh. Technol.* **2021**, *70*, 11433–11445. [[CrossRef](#)]
92. Jaguemont, J.; Boulon, L.; Venet, P.; Dube, Y.; Sari, A. Lithium-ion battery aging experiments at subzero temperatures and model development for capacity fade estimation. *IEEE Trans. Veh. Technol.* **2015**, *65*, 4328–4343. [[CrossRef](#)]
93. Wu, X.; Chen, Z.; Wang, Z. Analysis of low temperature preheating effect based on battery temperature-rise model. *Energies* **2017**, *10*, 1121. [[CrossRef](#)]
94. Ji, Y.; Wang, C.Y. Heating strategies for Li-ion batteries operated from subzero temperatures. *Electrochim. Acta* **2013**, *107*, 664–674. [[CrossRef](#)]
95. Ruan, H.; Jiang, J.; Sun, B.; Su, X.; He, X.; Zhao, K. An optimal internal-heating strategy for lithium-ion batteries at low temperature considering both heating time and lifetime reduction. *Appl. Energy* **2019**, *256*, 113797. [[CrossRef](#)]
96. Zhang, J.; Ge, H.; Li, Z.; Ding, Z. Internal heating of lithium-ion batteries using alternating current based on the heat generation model in frequency domain. *J. Power Sources* **2015**, *273*, 1030–1037. [[CrossRef](#)]
97. Ruan, H.; Jiang, J.; Sun, B.; Zhang, W.; Gao, W.; Ma, Z. A rapid low-temperature internal heating strategy with optimal frequency based on constant polarization voltage for lithium-ion batteries. *Appl. Energy* **2016**, *177*, 771–782. [[CrossRef](#)]
98. Jiang, J.; Ruan, H.; Sun, B.; Wang, L.; Gao, W.; Zhang, W. A low-temperature internal heating strategy without lifetime reduction for large-size automotive lithium-ion battery pack. *Appl. Energy* **2018**, *230*, 257–266. [[CrossRef](#)]
99. Qu, Z.G.; Jiang, Z.Y.; Wang, Q. Experimental study on pulse self-heating of lithium-ion battery at low temperature. *Int. J. Heat Mass Transf.* **2019**, *135*, 696–705. [[CrossRef](#)]

100. Wang, Y.; Rao, Z.; Liu, S.; Li, X.; Li, H.; Xiong, R. Evaluating the performance of liquid immersing preheating system for Lithium-ion battery pack. *Appl. Therm. Eng.* **2021**, *190*, 116811. [[CrossRef](#)]
101. He, F.; Li, X.; Zhang, G.; Zhong, G.; He, J. Experimental investigation of thermal management system for lithium ion batteries module with coupling effect by heat sheets and phase change materials. *Int. J. Energy Res.* **2018**, *42*, 3279–3288. [[CrossRef](#)]
102. Liu, F.F.; Lan, F.C.; Chen, J.Q.; Li, Y.G. Experimental Investigation on Cooling/Heating Characteristics of Ultra-Thin Micro Heat Pipe for Electric Vehicle Battery Thermal Management. *Chin. J. Mech. Eng.* **2018**, *31*, 179–188. [[CrossRef](#)]
103. Ruan, H.; Sun, B.; Zhu, T.; He, X.; Su, X.; Cruden, A.; Gao, W. Compound self-heating strategies and multi-objective optimization for lithium-ion batteries at low temperature. *Appl. Therm. Eng.* **2021**, *186*, 116158. [[CrossRef](#)]
104. Luo, M.; Lin, X.; Feng, J.; Ling, Z.; Zhang, Z.; Fang, X. Fast self-preheating system and energy conversion model for lithium-ion batteries under low-temperature conditions. *J. Power Sources* **2023**, *565*, 232897. [[CrossRef](#)]
105. Xu, J.; Mei, X.; Wang, H.; Wang, J. A Hybrid Self-Heating Method for Batteries Used at Low Temperature. *IEEE Trans. Ind. Inform.* **2020**, *17*, 4714–4723. [[CrossRef](#)]
106. Ruan, H.; Sun, B.; Cruden, A.; Zhu, T.; Jiang, J.; He, X.; Su, X.; Ghoniem, E. Optimal external heating resistance enabling rapid compound self-heating for lithium-ion batteries at low temperatures. *Appl. Therm. Eng.* **2022**, *200*, 117536. [[CrossRef](#)]
107. Wang, C.Y.; Zhang, G.; Ge, S.; Xu, T.; Ji, Y.; Yang, X.G.; Leng, Y. Lithium-ion battery structure that self-heats at low temperatures. *Nature* **2016**, *529*, 515–518. [[CrossRef](#)]
108. Yang, X.G.; Liu, T.; Wang, C.Y. Innovative heating of large-size automotive Li-ion cells. *J. Power Sources* **2017**, *342*, 598–604. [[CrossRef](#)]

**Disclaimer/Publisher’s Note:** The statements, opinions and data contained in all publications are solely those of the individual author(s) and contributor(s) and not of MDPI and/or the editor(s). MDPI and/or the editor(s) disclaim responsibility for any injury to people or property resulting from any ideas, methods, instructions or products referred to in the content.